Accepted for A.J. 3 May 02

Astrometry and Photometry for Cool Dwarfs and Brown Dwarfs

Conard C. Dahn, Hugh C. Harris, Frederick J. Vrba, Harry H. Guetter, Blaise Canzian, Arne A. Henden[1], Stephen E. Levine, Christian B. Luginbuhl, Alice K. B. Monet, David G. Monet, Jeffrey R. Pier, Ronald C. Stone, and Richard L. Walker
U.S. Naval Observatory, PO Box 1149, Flagstaff, AZ 86002-1149

Adam J. Burgasser[2]
Dept. of Astronomy and Astrophysics, UCLA, 8965 Math Sciences Bldg., Los Angeles, CA 90095-1562

John E. Gizis[3]
Dept. of Physics and Astronomy, University of Delaware, Newark, DE 19716

J. Davy Kirkpatrick
Infrared Processing and Analysis Center, MS 100-22, Pasadena, CA 91125

James Liebert
Steward Observatory, University of Arizona, 933 North Cherry Avenue, Tucson, AZ 85721

I. Neill Reid
Space Telescope Science Institute, 3700 San Martin Drive, Baltimore, MD 21218

ABSTRACT

Trigonometric parallax determinations are presented for 28 late type dwarfs and brown dwarfs, including eight M dwarfs with spectral types between M7 and M9.5, 17 L dwarfs with spectral types between L0 and L8, and three T dwarfs. Broadband photometry at CCD wavelengths ($VRIz^*$) and/or near-IR wavelengths (JHK) are presented for these objects and for 24 additional late-type dwarfs. Supplemented with astrometry and photometry from the literature, including ten L and two T dwarfs with parallaxes established by association with bright, usually HIPPARCOS primaries, this material forms the basis for studying various color−color and color− absolute

[1]Universities Space Research Association.

[2] Hubble Postdoctoral Research Fellow.

[3] NOAO WIYN Queue Investigator, Kitt Peak National Observatory, National Optical Astronomy Observatories. NOAO is operated by the Association of Universities for Research in Astronomy, Inc., under cooperative agreement with the National Science Foundation.

magnitude relations. The $I - J$ color is a good predictor of absolute magnitude for late-M and L dwarfs. M_J becomes monotonically fainter with $I - J$ color and with spectral type through late-L dwarfs, then brightens for early-T dwarfs. The combination of z^*JK colors alone can be used to classify late-M, early-L, and T dwarfs accurately, and to predict their absolute magnitudes, but is less effective at untangling the scatter among mid- and late-L dwarfs. The mean tangential velocity of these objects is found to be slightly less than that for dM stars in the solar neighborhood, consistent with a sample with a mean age of several Gyr. Using colors to estimate bolometric corrections, and models to estimate stellar radii, effective temperatures are derived. The latest L dwarfs are found to have $T_{\rm eff} \sim 1360$ K.

Subject headings: astrometry — color-magnitude diagrams — stars: brown dwarfs — stars: distances — stars: late-type

1. INTRODUCTION

The first identification of a low-mass dwarf cooler than the well-know M dwarfs came with the discovery of a very red companion to the white dwarf GD165 by Becklin and Zuckerman (1988). Initial spectroscopic observations at far-red wavelengths ($\lambda\lambda\,6300{-}9000$ Å) were puzzling because they showed none of the features characteristic of very late M dwarfs (Kirkpatrick et al. 1993). Subsequently, a faint companion to the bright M1V star Gliese 229 was discovered (Nakajima et al. 1995), and its near-IR spectrum was found to be dominated by deep absorption bands of methane (Oppenheimer et al. 1995), more similar to the planet Jupiter than to the known late-type, low-mass stars. The low luminosity of both objects could be measured through trigonometric parallaxes of their bright primary companions. Their spectra became prototypes for two new spectral classes, now designated L (having strong lines of neutral alkali elements and hydrides) and T (having strong bands of methane at near-IR wavelengths, and sometimes called "methane dwarfs"), both indicating cooler effective temperatures than type M (having strong molecular bands of TiO and VO). Several excellent papers review the rapid development of the observational data (Reid & Hawley 2000; Basri 2000; Liebert 2000) and theoretical understanding (Hauschildt et al. 1997; Chabrier & Baraffe 2000; Burrows et al. 2001) of these low-mass objects that bridge the gap between cool M stars and giant Jupiter-like planets.

Rapid growth of this topic has been spurred by the identification of *many* new L and T dwarfs from ongoing survey programs DENIS (Epchtein et al. 1997), 2MASS (Skrutskie et al. 1997), and SDSS (York et al. 2000). Initial results from DENIS (Delfosse et al. 1997) and 2MASS (Kirkpatrick et al. 1997a) revealed several objects which follow-up spectroscopy showed ranged from comparable to GD165B (DEN1058−15) to definitely cooler than GD165B, but definitely warmer than Gl 229B (DEN0205−11). By early 2000, the number of recognized L dwarfs had rapidly grown to nearly 100 (Kirkpatrick et al. 2000; hereafter, K00). However, the identification

of additional T dwarfs like Gl 229B proceeded much more slowly, despite considerable efforts searching for them. Finally, in mid-1999, several were identified, two by the SDSS collaboration (Strauss et al. 1999; Tsvetanov et al. 2000; Pier et al. 2000) and four by the 2MASS collaboration (Burgasser et al. 1999; Burgasser 2000c). As of this writing, a total of 30 T dwarfs have been found (Burgasser et al. 2002; a few not yet published).

As objects like GD165B became known, the logical first step in understanding this new population was to classify them into a spectral sequence. Kirkpatrick (1998) discussed at some length the need for one or more new spectral classes to accomodate objects cooler than the M dwarfs. He included "L" as a possible appropriate designation (see also Martín et al. 1997). Detailed classification systems were then developed independently by Martín et al. (1999c) and Kirkpatrick et al. (1999; hereafter, K99). The system proposed by Martín and coworkers is based on pseudocontinuum flux ratios in the red ($F_{\lambda 825nm}/F_{\lambda 756nm}$) calibrated to the temperature scale derived by Basri et al. (2000). Kirkpatrick's system maintains the spirit of the long standing MK classification scheme and is strictly morphological, relying on the progressive strengthening and weakening of various spectral features and ratios within the $\lambda\lambda$6300–10000 Å window from $\sim$10 Å resolution spectra. The two scales agree on average for earlier types through about L2V (although they often disagree for individual objects), but diverge for later types, with L7.5V on the Kirkpatrick scale corresponding roughly to L6V on the Martín et al. scale.

Similarly, the Gl 229B-like objects have been grouped together into a spectral class designated as "T," following the proposal by Kirkpatrick (K99). Classification by the 2MASS group (Burgasser et al. 2002) uses indices measuring the strengths of the CH_4 bands at 1.3 and 1.6 μm, the H_2O/CH band blend at 1.15 μm, along with the flux peak ratios between the zJK bands, from lower resolution (R$\sim$100 at 1 μm) spectra. Classification by the SDSS collaborators (Geballe et al. 2002) employs higher resolution spectra (R$\geq$ 400), measuring indices sensitive to the H_2O and CH_4 bands at $\lambda\lambda$ 1.15-2.2 μm, but the results are in excellent agreement with those from the 2MASS group (with a maximum difference of only one-half spectral subclass for 11 stars in common to the two studies). Efforts to classify L dwarfs and the L/T transition objects from near-IR spectra have been made by several groups (Reid et al. 2001; Testi et al. 2001; Geballe et al. 2002; McLean et al. 2002). Results from these studies made at different spectral resolution and their correlation with classification made from optical spectra are not yet understood completely.

With several classification schemes defined, the present challenge is to better understand the atmospheric physics responsible for the various spectral features. Evaluating the spectral sequences in terms of $T_{\rm eff}$ is perhaps the most basic. A rough scale (K99) for the late-M through L dwarfs based on the observed appearance/disappearance of various far-red ($\lambda\lambda$ 0.63–1.01 μm) spectral features compared with the theoretical atmosphere models of Burrows and Sharp (1999) runs from $T_{\rm eff}\sim$2000 K at L0 to $\sim$1500 K at L8. Martín et al. (1999c) established their L-dwarf spectral classification sequence to correspond to a temperature sequence running from 2200 K at L0 to 1600 K at L6 (or $\sim$L7.5 on the Kirkpatrick system), with $T_{\rm eff}$ values primarily from the work of Basri et al. (2000). The rapid development of model atmospheres for such cool dwarfs has

aided the interpretation of spectroscopic data, and several other studies have made temperature estimates (e.g. Pavlenko et al. 2000; Leggett et al. 2001; Stephens et al. 2001; Schweitzer et al. 2001, 2002). However, creating realistic models is challenging, particularly in the treatment of dust. At present, discrepancies exist between the models and observed spectra, leaving some doubt that current model atmospheres alone can be used to provide accurate effective temperatures. However, effective temperatures of cool dwarfs are closely related to their luminosities because (with the exception of young objects, with ages < 0.3 Gyr) they have only a small range of radii, set by the equation of state of their degenerate interiors. This alternate method for determining their temperatures from their luminosities was first used by K00, and is a motivation for measuring parallaxes for additional cool dwarfs. Temperatures determined for a few late-L dwarfs from luminosities tend to be systematically lower than those determined from a comparison to model atmospheres (Leggett et al. 2001; Schweitzer et al. 2002). There is presently a significant range in the various temperature scales for late-M through late-L dwarfs (Chabrier 2002).

Distance measurements are needed to determine the luminosities of individual objects. More than that, several factors make it necessary to measure an ensemble of cool dwarfs of a given type in order to acquire their mean luminosity (and range of luminosities), to identify outliers, and to establish observationally the luminosity of their isochrones. First, any measured dwarf can always be an unresolved binary, with colors and magnitudes measured for the composite system. Second, field dwarfs with extreme ages can have atypical luminosities for their color, temperature, or spectral type. Third, very cool dwarfs may exhibit a wider range of observational characteristics than do warmer main sequence stars due to the presence and variation of dust opacity. Simple models (e.g. Burrows et al. 2002; Marley et al. 2002) predict a sensitivity of colors for different surface gravity, metallicity, and dust precipitation, and the near-IR colors of L dwarfs (e.g. Leggett et al. 2002a) show little correlation with spectral type. Fourth, temporal variability is also expected if atmospheric clouds change with time. Observations to date indicate only low-level variability (e.g. Bailer-Jones & Mundt 2001), but larger amplitudes may occur for some objects.

Substellar brown dwarfs are being studied in young clusters, but in intermediate-age or old clusters they are too faint and rare to provide useful samples. A few very cool dwarfs (like GD165B and Gl 229B mentioned above) are companions of brighter stars, where the parallax of the brighter primary star can be easily measured. There are insufficient numbers of these, however, to draw general trends. Therefore, we are left with the need to measure trigonometric parallaxes for a substantial number of field L and T dwarfs. In this paper, we extend previous work (K00; Dahn et al. 2000) by presenting parallax measurements for eight M, 17 L, and three T dwarfs. Together with companions to brighter stars with parallaxes already available, there are now 25 L dwarfs compiled in this paper, enough to establish their isochrones with some reliability for the first time. Only five T dwarfs have known distances, so for them the work is just beginning.

2. ASTROMETRY

2.1. Observational Procedures

The astrometric observations reported here were carried out as part of the Naval Observatory CCD faint-star parallax program using the 1.55 m Strand Astrometric Reflector. The camera (designated TEK2K and used for all fields except LP412−31) employs a thinned, back-side illuminated Tektronix 2048 x 2048 CCD with 24.0 micron pixels, corresponding to 0.325 arcsec pix^{-1}. This scale gives a field of view of 11 x 11 arcmin. The LP412−31 parallax observations presented here were made during the time period 1990.8 to 1995.8 using a thinned Texas Instruments 800 x 800 CCD (TI800). This camera system and wide-R filter have been described in detail by Monet et al. (1992).

Beginning in late 1992, the entire USNO faint-star parallax program began transitioning to the larger format TEK2K camera due to the availablity of improved reference star frames within the larger field of view. As a result of experience gained with the TI800 camera, the TEK2K chip is mounted on the 1.55 m with the columns oriented (to a high accuracy) east-west. This orientation takes advantage of the fact that slightly higher astrometric accuracy appears to be obtained along CCD columns versus CCD rows, and the fact that the larger annual parallactic shift occurs in Right Ascension. At the time that the TEK2K observations for these fields were initiated, the reddest astrometrically flat filter available was a wide-I interference filter with passband centered at $\sim$8100 Å and with FWHM $\sim$ 1910 Å. Consequently, the majority of the fields have been observed with this filter. In response to the difficulties encountered in attempting to observe the extremely red T dwarfs using the 1.55 m and this I filter, an astrometrically flat SDSS z^* filter was procured in 1999. This z^* filter plus CCD detector gives a passband centered at roughly $\sim$8800 Å and with FWHM $\sim$ 1100 Å. It has been employed for the astrometry of the three T dwarfs presented here and for the L dwarf 2MW0825+21; the wide-I filter has been employed for all of the other TEK2K fields.

Experience carrying out parallax astrometry with TEK2K on over 200 fields for epoch spans as long as 9 years demonstrates that relative astrometric measurements accurate to $\sim \pm 3$ mas are routinely obtained for a single, well-exposed, image. Although the quality of a parallax determination depends on many factors, including the quality of the available stellar reference frame and particularly on the observational coverage of the parallactic ellipse, a formal standard error for the relative parallax of $\sim \pm 0.5$ mas is typically realized with TEK2K after roughly 100 observations adequately distributed over the parallactic ellipse and spanning at least three years in epoch range. However, many of the targets in the present sample are far from "typical." In fact, several of these objects (e.g., PC0025+04, 2MW0850+10, 2MW1328+21, SDSS1624+00, and 2MW1632+19) are so faint that nearly ideal observing conditions – cloudless, dark skies (moonless and well away from twilight), and with seeing better than 1.2-1.4 arcsec FWHM – are required to secure astrometrically useful data; and even then the exposure times required are 60–90 min in length for only relatively low S/N results. Together with seasonal weather patterns, these constraints result in less than ideal coverage of the parallatic ellipse and, as we shall see below, much less accurate parallax determinations than those obtained for brighter stars when using

TEK2K.

The observing procedures employed in the TEK2K parallax program call for exposures to be centered within ± 15 min of meridian transit. Strict adherence to this rule effectively eliminates the need for a correction for differential color refraction (DCR; cf. Monet et al. 1992). This is because astrometry for purposes of parallax determinations is highly differential – all that we are interested in is the shift in position as a function of time produced by different parallax factors as the Earth orbits the Sun. By taking all observations close to meridian transit (at constant hour angle and, hence, constant zenith distance) the shift in position of the target star relative to the reference stars caused by DCR is, to first-order, identical for all observations on any particular target. This is especially advantageous for astrometry of targets as extremely red as the L and T dwarfs presented here. As a matter of routine, a DCR correction has been applied to the L dwarfs observed with the wide-I bandpass if the $V - I$ colors of the reference stars have been measured (i.e., for all L dwarf fields except 2M1658+70 and 2M2224-01), although the calibrated correction must be extrapolated considerably for the mid- to late-L dwarfs. This correction allows for small, second-order DCR effects resulting from the fact that the exposures are not centered *exactly* on meridian transit. Examination of the solutions carried out both with and without the DCR correction reveals at most differences of a few tenths of a mas in the derived relative parallaxes. A DCR correction for the z^* filter has not yet been calibrated, although the effects are expected to be smaller than the effects in the I filter because atmospheric dispersion is reduced. Hence, particular care has been taken to examine the parallax determinations for the four fields observed in z^* by carrying out solutions including a DCR term within the formal least-squares algorithms and by examining the residuals to parallax results as a function of the projected tangent of the zenith distance at the times of individual observations (cf. Monet et al. 1992). The effects of DCR are less than 0.3 mas in the parallax for these four objects.

2.2. Present Results

Table 1 presents the astrometric results for the 28 targets. The first column in Table 1 contains abbreviated names of the objects, also used throughout the text. The objects in Table 1 (as well as those in Tables 2 and 3 following) are presented in order of increasing right ascension. Full names, coordinates, and references for all objects in Tables 1-3 are given in the Appendix. The first column also contains the spectral classification on the system established by Kirkpatrick and co-workers (Kirkpatrick et al. 1991; Kirkpatrick et al. 1995; K99; Burgasser et al. 2002). The second column in Table 1 summarizes the data employed in each parallax determination presented here: the total number of observations (CCD frames) and the epoch range in years between the first and last observations. The third column gives the derived relative parallax and formal standard (mean) error, while the fourth column gives the absolute parallax allowing for the

finite distance of the reference stars[4]. The fifth and sixth columns give the total relative proper motion and position angle of that motion (measured in the conventional sense of north through east) obtained from the simultaneous least-squares solutions to the observations, along with their formal uncertainties. There is no simple and direct method for correcting our derived relative proper motions to absolute (i.e., to a quasi-inertial reference frame). For reference objects as faint as those employed for the majority of the present targets, we expect such corrections to be less than a few mas per year. Since most of the 28 objects in Table 1 have measured relative proper motions in excess of 100 mas yr^{-1} (the noteable exceptions being PC0025+04 and, to a lesser extent, T513−46546 and 2M0326+29), the resulting uncertainties for kinematic analyses are not large. The seventh column contains the tangential velocities (with respect to the Sun) calculated from the absolute parallaxes and the relative proper motions given in the fourth and fifth columns, respectively.

Most of the astrometric solutions presented in Table 1 are "preliminary" in the sense that these fields are still being observed on a regular basis. The exceptions are CTI0126+28, LP412−31, T213−2005, T513−46546, and GRH2208−20 which are no longer being observed and, therefore, the tabulated determinations are considered "completed." Inspection of Table 1 reveals that some fields have been observed for a long period of time – over 9.1 years in the case of PC0025+04 – while others have been observed for only a short time – only 1.2 years in the case of SDSS1254−01. Parallax determinations from short time series of observations in particular must be regarded with some suspicion.

2.3. Reliability Checks

We routinely employ two methods to judge the reliability, or robustness, of our parallax determinations. The first is based on experience gained from the examination of over 230 TEK2K parallax solutions for over 220 different fields, including nearly a hundred with five years or more of data coverage. From this ensemble of solutions we know how the derived parallaxes and their formal mean errors are expected to behave as a function of time from the point that solutions are first possible (i.e., when the change in Right Ascension parallax factor becomes non-monotonic)

[4] The formal least-squares reduction algorithms set both the mean parallax and the mean proper motion of the reference stars employed in each field identically equal to zero. The corrections from relative to absolute parallax employed here were derived from photometrically determined distances to the individual reference stars using the same VI photometry employed for the DCR corrections. As can be seen by comparing the entries in the third and fourth columns, the mean distances of the reference frames are typically between one and two kiloparsecs, and the uncertainty in this correction is only rarely large enough to increase the uncertainty of the derived absolute parallax. For the six fields lacking reference star photometry to date (the four z^*-filter fields plus 2M1658+70 and 2M2224−01), a correction to absolute parallax of 0.8 ± 0.2 mas has been adopted based on similarly faint reference star frames located at comparable galactic latitudes and with photometrically derived mean distances. Note that all but one of these six targets (2M1658+70) is found to lie within 12 pc of the Sun, so that small uncertainties in the correction to absolute parallax only compromise luminosity determinations derived from these parallaxes at the 0.01 mag level.

and then as data frames are accummulated one by one. These results have demonstrated that (1) after about 2 years of observations individual solutions generally remain very stable, and (2) the actual parallax value derived from that point on agrees – to within the formal error at any particular time – with the "completed" determination. The formal error becomes smaller with time as data are added to the solution, of course, and falls approximately as $N^{-1/2}$, where N is the number of CCD frames in the solution. Generally, the error in the parallax determination at the time the star is removed as "completed" is some minimum value that is approached quasi-asymptotically. The actual value of this error is very much field-dependent due to many factors including the quality of the reference star field available and especially the coverage of the observations over the parallactic ellipse. In general, for a typical TEK2K field little improvement in parallax precision is achieved with observations extending longer than about five years.

As a second check we routinely examine and compare the two separate (but not truly independent, since the same data frames are employed) solutions for parallax that are derived from image displacements in RA and DEC, respectively. Maintaining these two solutions separately and only combining them into a weighted mean relative parallax as a final step preserves useful diagnostic information regarding contamination by (nearly) unresolved field stars, DCR problems, or perturbations from unresolved physical companions. While the range of parallax factor in DEC covered by the observations is usually less (and frequently very considerably less) than realized in RA, we should expect the two solutions to agree with one another to within the combined errors of the two. For all of the solutions presented in Table 1, the individual RA and DEC parallax solutions agree satisfactorily – that is, usually to within their combined errors and no worse than 1.2 times that amount.

Very preliminary parallax results were presented for 12 of the objects in Table 1 at the "Giant Planets to Cool Stars" conference held in June 1999 at Northern Arizona University (Dahn et al. 2000) and slightly updated values were employed in Table 3 of K00. Since that time some investigators have expressed skepticsm about these values due to the lack of DCR corrections for such extremely red targets (Martín et al. 1999a) or due to the short epoch coverage of the data ($\sim$1 year) for some fields. As mentioned above, restricting our observing close to times of meridan transit effectively eliminates DCR as an issue. Comparisons of the Table 1 values with the earlier (1999) results demonstrate agreement that is at least satisfactory and in most cases good to excellent, except for PC0025+04 and DEN0205−11 which are discussed further in the following section.

Direct comparison of the present parallaxes with independent determinations from other observatories are only available for three of the objects in Table 1. Tinney et al. (1995) presented parallax results based on CCD observations from the Palomar 1.5 m reflector for these three objects. For T832−10443, the agreement is excellent – Pi(abs) = 36.4 ± 3.0 from Tinney et al. versus Pi(abs) = 36.0 ± 0.4 mas from this paper. For T513−46546 the agreement is less satisfactory – Pi(abs) = 101.8 ± 5.2 mas from Tinney et al. versus Pi(abs) = 93.2 ± 0.5 from this paper. However, the Tinney et al. determination is based on observations spanning less than

1.6 years and the formal error of their result is quite large. The present result for T213−2005 – Pi(abs) = 29.3 ± 0.4 mas – does not agree well the Tinney et al. determination of Pi(abs) = 53.2 ± 4.5 mas. Tinney et al. note that an anomalously large difference existed between their relative parallax solutions in RA and DEC, and suggested that unresolved duplicity might explain this discrepancy. The Table 1 solution, which is based on observations covering an epoch range of 7.0 years, shows no sign of a perturbation and the separate RA and DEC solutions agree satisfactorily with one another (29.0 ± 0.4 mas versus 30.8 ± 1.0 mas).

2.4. Comments on Individual Targets

The parallax determination for PC0025+04 has been particularly troublesome and after 9 years of observations the solution remains quite fragile. The formal error for the relative parallax has still only come down to 1.6 mas. Undoubtedly, this is due primarily to the faintness of this target. Earlier solutions yielded preliminary parallaxes for PC0025+04 from as high as 17 mas down to about 13 mas, depending on what criteria were adopted for rejecting lower-S/N data. The solution presented in Table 1 employs the maximum data possible; that is, only data frames very obviously bad have been rejected here. The fact that the proper motion position angle of PC0025+04 (∼ 95 deg) is quite closely aligned in an east–west direction where the majority of the parallactic shift occurs, and that the size of the annual proper motion is comparable with the annual parallactic shift, undoubtedly contributes to difficulties in simultaneously solving for these two quantities from low S/N data, especially for observations extending over a short epoch range. However, for observations covering 9 years, we would expect the signals due to parallax and proper motion to be well separated by now. The Table 1 parallax now places it above the loci of other points in various absolute magnitude versus color diagrams (see Fig. 4 below), suggesting the possibility that this is an unresolved binary system (Burgasser et al. 2000a). The residuals from our astrometric solution only allow us to rule out perturbations with amplitudes larger than about 1 mas and for periods in the 2 to 7 year range. Shorter periods would not be resolved in our limited, low S/N data. Martín et al. (1999a) discussed the status of PC0025+04 in detail and reported no radial velocity variability in observations on nine nights covering 3.1 years. However, they detected Hα emission, variable but consistently high (EW∼ 100–400 Å), and may have detected LiI λ 6708 Å absorption (EW=1.0±0.3 Å). The absolute magnitude derived from our most recent astrometry seems at least qualitatively consistent with the Martín et al. conclusion that PC0025+04 is probably a young (<1 Gyr) object.

The 1999 parallax solution for DEN0205−11 (59.4 ± 2.6 mas) differs quite significantly from the current (Table 1) value of 49.8 ± 1.5 mas. Examining the evolution of the solution to date reveals that, while the error in the parallax has been decreasing with time, so too has the parallax itself. DEN0205−11 is now known to be a close (Sep. ∼ 0.4–0.5 arcsec) binary pair (Koerner et al. 1999), but since the components have equal brightnesses at JHK bandpasses (Leggett et al. 2001), a reasonable assumption is that they also have equal brightnesses at the I-band employed

for our astrometric observations. If this is the case, then the center of light is very likely coincident with the center of mass of the system and our parallax astrometry should not be affected. Our observational coverage of the parallactic ellipse is not particularly good for this field and this may have been a problem for the 1999 solution whose observations included only 1.2 years of epoch coverage.

The 1999 results for 2M0149+29 were based on an epoch range of only 0.4 years and were presented to demonstrate that under favorable conditions (i.e., intense observational coverage) meaningful results could be obtained even when the change of the parallax factor in RA was still monotonic – *if* that change were sufficiently non-linear with time. The present astrometry shows residuals in both the individual RA and DEC solutions that hint at a possible perturbation. However, it is premature to conclude that this is an unresolved binary system. Liebert et al. (1999) discuss the variability in the spectra observed for 2M0149+29 and compare the Hα activity with that observed for PC0025+04, concluding that 2M0149+29 is more like a single object which exhibits spectacular flaring. For further discussion here we will assume that 2M0149+29 is single; but we will continue to monitor the astrometry for evidence of a perturbation.

3. PHOTOMETRY

For very cool dwarfs, broad-band photometry at near-infrared wavelengths is primarily sensitive to the strong molecular bands of H_2O, CH_4, CO, and H_2. Broadband photometry at "optical" wavelengths ($\lambda \leq 1\mu$) measures very different spectrophotometric features. Despite the faintness of cool dwarfs, optical photometry is potentially useful as diagostic of the stellar temperature, surface gravity, metallicity, and the dust content of the photosphere (e.g. Marley et al. 2002; Burrows et al. 2002). In this section, we present both optical and near-IR photometry in order to explore (in the following section) different color-magnitude diagrams, seeking colors that are most sensitive to the physical properties and evolutionary state of the objects. New photometric data are presented in Table 2. Data from the literature are summarized in Table 3.

3.1. New Optical Photometry

We have chosen to measure V, $R_{\rm C}$, $I_{\rm C}$, and z^* where possible, and to transform data from the literature to these passbands where practical.[5] These bands cover the red portion of the optical spectrum, and extensive photometry of dM stars already is available in the VRI filters. The $I_{\rm C}$

[5] Here V is on the Johnson system, $R_{\rm C}$ and $I_{\rm C}$ are on the Cousins system, and z^* is on the SDSS system. The z^* (and other) SDSS magnitudes have zeropoints defined to be on an AB magnitude system, while VRI and the infrared JHK data described below have zeropoints chosen to give Vega-like stars colors of zero. Combining these different magnitudes into colors like $I_{\rm C} - z^*$ or $z^* - J$ is legitimate if it is done consistently.

filter is strongly affected by the KI resonance doublet lines in late-L and T dwarfs, making $I - z^*$ and $I - J$ colors even more sensitive to the steepening slope of the optical continuum at late spectral types than they would otherwise be. The R_C filter is also affected by the KI lines. The V filter is strongly affected by the NaI resonance lines.

Obtaining accurately-calibrated photometry for objects that are much redder than any photometric standard stars requires some care. Most of the measured flux in $VRIz^*$ filters for late-M, L, and T dwarfs comes from the few hundred Å at the red end of each passband, whereas the measured flux for standard stars comes from the entire passband. Therefore, non-linear color terms are to be expected when calibrating instrumental magnitudes. Photometry taken with different photometric systems can be transformed to other systems, but the corrections will be large when the red cutoffs of the filters are very different. For example, SDSS i^*, Cousins I_C, Thuan-Gunn i, and HST F814W are similar filters, primarily measuring the flux redward of the KI lines, but their red edges (at 8180, 8820, 8700, and 9600 Å, respectively) are sufficiently different that a late-L dwarf will be measured differently by 2.4 mag between the extreme two of these four filters, as we discuss below.

The new optical photometry presented in Table 2 includes all 28 objects from Table 1 plus 24 additional cool dwarfs with distances already known or that will be useful in exploring the color–spectral type diagrams. The new photometry was obtained primarily with the USNO 1.0 m telescope on 28 nights during 1998-2000. Some z^* observations of the faintest objects were made with the USNO 1.55 m telescope. Data (or lower limits) in V and R_C for six objects (2M0850+10, 2M1328+21, 2M1553+21, 2M1632+19, 2M1726+15, and 2M2101+17) were obtained with the WIYN[6] 3.5 m telescope on six nights in 1999. All VRI data were reduced using Landolt (1983, 1992) standards, always including stars with a wide range of colors, typically $V - I$ of 0.4-2.4 or greater range. Nightly measurements were made for extinction and color terms. For the faint program objects, sometimes only one filter was observed on a given night, and the color terms were applied using observations in another filter from a different night in a bootstrap procedure. Transformations of the form

$$I = i - a_0 - a_1 X - a_2(R - I) - a_3(R - I)^2$$

(and similar for the other filters), where X is the airmass, were used to correct instrumental magnitudes to the standard system. The V and R glass filters and the I interference filter used at USNO are close to the standard passbands, but do not match exactly. As mentioned above, the red cutoff of each passband is of primary importance for the red program stars in this paper. The red side of the passbands for our filter/detector cameras are about 60 Å too red, 200 Å too blue, and about 250 Å too red, respectively, compared to the V, R, and I passbands tabulated by Bessell (1990a); the color terms in the transformations account for these differences. We find

[6] The WIYN Observatory is a joint facility of the University of Wisconsin-Madison, Indiana University, Yale University, and the National Optical Astronomy Observatories.

good systematic agreement with data from Bessell (1990b) for M stars, although some stars have larger differences than expected that could be due to stellar variability. See Monet et al. (1992) for a comparison of USNO photometry with data from other sources. For L and T dwarfs, there is little other optical photometry with which to compare.

The z^* filter, CCD, and telescope used for most of the z^* observations in this paper are the same used to set up the preliminary SDSS standard-star network. Observations presented here were reduced using preliminary standard values for the standard stars taken from Smith et al. (2002), applying nightly extinction values but no color terms. Therefore, these data should be on the standard-star system with good accuracy despite a limited range of color for the observed standard stars. However, the SDSS system will ultimately be defined by the survey camera on the SDSS 2.5 m telescope, where the red side of the z^* passband is defined by the sensitivity of the six thick CCDs with z^* filters in that camera. The SDSS observations reported to date for L and T dwarfs in several papers are on a preliminary system not yet tied to the system of standard stars with color terms, as they eventually will be. Measurements of the QE of the z-band CCDs in the SDSS survey camera indicate that they do not have as much sensitivity at wavelengths beyond 10500 Å as had been expected for thick CCDs; thus, fortuitously, they match the sensitivity of the CCD in the USNO camera quite well. Data in Tables 2 and 3 (see Sec. 3.3 below) for five objects observed with both telescopes show this agreement as well: the differences (USNO-SDSS) for SDSS0330−00, SDSS0413−01, SDSS0539−00, SDSS1254−01, and SDSS1624−00 are -0.05 ± 0.05, 0.00 ± 0.04, -0.03 ± 0.02, $+0.05\pm0.06$, and -0.13 ± 0.06, respectively. Therefore, the z^* data in Table 2 are taken to be on the preliminary SDSS z^* system until a final SDSS photometric system is established.

3.2. New Infrared Photometry

The $J-H$, $H-K$, and K colors and magnitudes presented in Table 2 were obtained with the IRCAM imager at the 1.55 m Strand Astrometric Reflector at USNO, Flagstaff Station. IRCAM employs a 256 x 256 HgCdTe NICMOS III array pixelized at $0.54''$ pix^{-1}. The numbers of independent observations, on different nights, are given in the last three columns. Each observation of a program object consisted of three or four images, each with several minutes of integration, taken at dithered positions of the telescope, even for the brightest objects. On each night of observation between 10 and 22 standard stars were observed in order to determine nightly extinction coefficients and color terms. The standards were selected from the list of Elias et al. (1982) and thus place the resulting photometry on the CIT system. Most data were reduced to the standard system in terms of the $J-H$ and $H-K$ colors and K magnitude. For a few objects noted in Table 2 with noisy or missing H or K data, the J magnitudes were reduced and reported separately. The IRCAM JHK filters are well-matched to the CIT standard system with mean deviations from 1.0 in the transformation slopes from instrumental to standard colors <1% for $J-H$ and $H-K$. No $J-K$ color term was ever found for the K magnitude instrumental to

standard value offset.

We add the caveat to the USNO photometry results that the standards used above only extend to red colors of approximately $(J - H,\ H - K) = (0.81,\ 0.36)$; roughly that of a main sequence mid- to late-M star. For the redder late-M and L dwarfs measured here, colors have been derived by extrapolation beyond the range of the previously derived standard system.

3.3. Additional Photometry

Many late-M, L, and T dwarfs also have JHK photometry available in the literature, particularly from 2MASS, that can be used to supplement the data in Table 2. The recently introduced MKO-NIR system (Tokunaga et al. 2002) also has been used for observing L and T dwarfs (Leggett et al. 2002a). A detailed comparison of these different systems is beyond the scope of this paper. In Figure 1, we make a comparison for late-M through L dwarfs, comparing USNO data on the CIT system (Table 2) with 2MASS photometry (left panels) and with MKO photometry (right panels). These comparisons do not include T dwarfs, which are expected to behave differently. Both 2MASS and MKO filters have passbands different from the CIT-system filters, so some systematic differences are to be expected [7]. Carpenter (2001) finds only a very small difference between 2MASS and CIT J magnitudes, including several red standards (but not including L or T dwarfs). Figure 1 suggests that for late-L dwarfs the 2MASS J magnitudes are systematically fainter than the CIT J magnitudes; the five reddest objects have a mean difference of 0.14 ± 0.06, formally significant, but obviously not well-determined. Because many L dwarfs have been discovered with 2MASS data using a selection for objects with $J - K$ colors redder than some limit, a bias may exist in the J and K 2MASS magnitudes for those faint L dwarfs discovered by 2MASS (K00). Therefore, some of the difference in J magnitudes seen in Figure 1 may be a result of this selection procedure. Because this difference is small and of an uncertain amount, no corrections to 2MASS data have been applied in the following section. However, the MKO system is significantly different from both the 2MASS and CIT systems, resulting in color corrections for M, L, and T dwarfs (Leggett et al. 2002a). We therefore avoided its use in our analysis.

Table 3 gives the additional data used, where a weighted mean has been adopted for objects with data from more than one source, including objects listed in both Tables 2 and 3. For near-infrared data, we made use of 2MASS photometry from K99, K00, Gizis et al. (2000), Burgasser (2001), and Wilson et al. (2001). The comparison of 2MASS and CIT photometry was described above. We also included UKIRT photometry (not on the MKO-NIR system; see Leggett et al. 2002a) in our adopted values for the two T dwarfs SDSS 1346−0031 (K data only,

[7]Note that 2MASS data are reduced using CIT-system standard stars, but without application of color terms, thus effectively making the 2MASS photometric system unique.

from Tsvetanov et al. 2000; J and H adopted values are on the CIT system listed in Table 2) and Gl 229B (JHK data, from Leggett et al. 1999); UKIRT-system values are expected to be somewhat different from the CIT and 2MASS values used elsewhere in this paper, but are the only data presently available for these two stars. I_C photometry for 2M1217−03, 2M1237+65, SDSS1346−00, SDSS1624+00, 2M1726+15, 2M2101+17, and Gl 570D was synthesized from spectral data from K00 and Burgasser et al. (2000b; 2001), and z^* photometry for Gl 570D was synthesized from combined spectral data from Geballe et al. (2001) and Burgasser (2001).

Spectrophotometric colors for Gl 229B at I_C and z^* could not be directly obtained due to the short wavelength cutoff of the Oppenheimer et al. (1998) spectrum (flux calibrated by Leggett et al. 1999). Therefore, we obtained this photometry by applying color corrections to the Gunn i and z measurements from Nakajima et al. (1995) and HST F814W and F1042M measurements from Golimowski et al. (1998). These corrections were synthesized from optical and near-infrared spectra of mid-type T dwarfs from Burgasser (2001) and Geballe et al. (2002). We were careful to include the quantum efficiency (QE) of the CCD detectors used for the photometric measurements, particularly in the z band where the CCD QE decay at long wavelengths cuts off the otherwise long-pass Gunn and Sloan filters. We derive $I_C = 20.5\pm0.3$[8] and 19.92±0.14 from the Gunn i and F814W magnitudes, respectively, which are marginally consistent within the uncertainties. We adopt the HST-derived magnitude value for the remainder of the paper. For z, we derive $z^* = 20.0\pm0.3$ and 17.69±0.07 from the Gunn z and F1042M magnitudes, which are clearly inconsistent. The mean Gunn z-F1042M color measured from the spectra of SDSS 1624+0029 and SDSS 1346-0031 (both classified T6; Gliese 229B is classified T6.5 by Burgasser et al. (2002)) is 1.54±0.13, as compared to 3.8±0.3 from the photometry. Because the HST F1042M-F814W color for Gl 229B is consistent with the spectral data, we conclude that the Gunn z measurement from Nakajima et al. (1995) is descrepant by over 2 mags, possibly due to its significant sensitivity to the properties of the CCD detector. We therefore adopt the HST-derived value for z^*. This exercise again emphasizes the need for careful photometric calibration of L and T dwarfs at these wavelengths, due to their significant spectral slopes at $\lambda\lambda$8000-11000 Å.

4. DISCUSSION

4.1. Absolute Magnitude–Spectral Type Relations

The parallax values in Tables 1 and 3 and the photometry in Tables 2 and 3 give the absolute magnitudes in each passband. Five objects are known to be resolved binaries.[9] For these binaries, photometry in the tables is given for the combined light, so the magnitudes for the individual

[8]Uncertainties are derived from the original measurements and scatter in the color correction.

[9] One additional object, 2M0345+25, was suggested to be a double-lined spectroscopic binary (Reid et al. 1999), but reexamination of the data indicates that that the object is more likely single with broad lines.

components have been calculated as follows. For two objects (DEN0205−11, and DEN1228−15), the components are observed to have equal or nearly equal magnitudes at JHK (Koerner et al. 1999; Martín et al. 1999b; Leggett et al. 2001). They are assumed to be identical objects with each component being 0.75 mag fainter than the combined light at all bandpasses. For three other dwarfs (2M0746+20, 2M0850+10, and 2M1146+22), the magnitude difference between the components has been measured with the F814W filter on HST and the magnitude difference in J has been estimated by Reid et al. (2001b). Using the observed color-color plots for L dwarfs described below, we have made estimates of the magnitude difference in other passbands, including error estimates allowing for the scatter seen in JHK colors for L dwarfs and the unknown (late-L or T) spectral type of 2M0850+10B. The estimated magnitude differences are listed for these three binaries in Table 4. From these values and the photometry for the combined light given in Tables 2 and 3, the magnitude of each component in each filter can be calculated, and is used for plotting in the figures.

Figure 2 presents M_I, M_J, and M_K as a function of spectral type. Spectral types are on the system established by Kirkpatrick and co-workers, as described in Sec. 2.2. They are accurate within that system to typically one-half spectral subtype or better. All three diagrams show clear monotonic relations from mid-M through late-L with a nearly linear slope. There is some scatter in these relations with a range of ± 0.5 mag; this scatter is significantly greater than the measurement uncertainty and, hence, is likely due to both cosmic scatter (age, metallicity, etc.) and possible binarity. There is a clear break in this relation as we cross into the T dwarf regime, however. Both SDSS1254−01 (T2) and 2M0559−14 (T5) have M_I and M_K values that are similar to the latest L dwarfs, and 2M0559−14 is more than a magnitude brighter at J than the L8 dwarfs. Even if this object is an equal-magnitude binary (despite it being unresolved in HST images – Burgasser 2001), then both M_I and M_K show a moderate dimming from L8 to T5, while M_J shows a moderate brightening from L8 to T5, followed by all magnitudes rapidly dimming for late-T dwarfs to Gl 570D at T8. This pattern could be consistent with substantial flux redistribution toward J as these objects cool, causing M_J to brighten temporarily even as the bolometric luminosity is decreasing (see Sec. 5). Alternatively, the unexpected bright magnitudes of 2M0559−14 may be a symptom of more complicated behavior in early-T dwarfs, and a real dispersion in luminosities as large or larger than that seen in L dwarfs. Distances for more T dwarfs are urgently needed to address this issue.

4.2. Spectral Type–Color Relations

In Figure 3, a selection of optical colors are plotted as a function of spectral type, and Figure 4 shows $I - J$ and $J - K$ against spectral type. In general, the optical colors grow redder with increasing spectral type. The $R - I$ and $I - z^*$ colors are nearly constant from M8 through L4 spectral types, as has been previously noted (Fan et al. 2000; Steele & Howells 2000; Schneider et al. 2002) while $V - I$ and $z^* - J$ are increasing. With a few exceptions, $I - z^*$ shows very little

scatter at a given spectral type. Notable outliers are PC0025+04 (M9.5) and 2M1841+31 (L4), both with peculiar spectra, and GD165B (L4) which may have its I magnitude corrupted by its brighter primary. Probably $R-I$, $I-z^*$, and spectral type are all heavily influenced by the relative prominance of molecular bands (TiO and VO) vs. atomic (KI) absorption in late-M through mid-L dwarfs. $I-J$ appears to be good diagnostic of spectral type, increasing monotonically from mid-M to late-T, but with more scatter than $I-z^*$. There is a change in slope between the late-M dwarfs and L dwarfs, with $I-J$ colors increasing less rapidly in the latter objects. In the latest L dwarfs and T dwarfs, $I-J$ color is heavily influenced by KI absorption, and the increased reddening is consistent with the observed (Burgasser 2001) and predicted (Burrows et al. 2002) strengthening of the $\lambda\lambda$ 8000–11000 Å slope for these spectral types. As discussed in Burrows et al. (2002), the strength of KI absorption is also heavily dependent on gravity and metallicity, a fact that may explain the significant scatter seen in some L and T dwarfs.

$J-K$ color trends in M, L, and T dwarfs have been examined by a number of authors, and we see similar behavior in the bottom, right-hand panel of Figure 4: reddening from M to L, likely caused by dust, followed by a significant change to blue near-IR colors in the T dwarfs where CH_4, H_2O, and CIA H_2 opacity dominate. Note the significant scatter in colors between spectra types L2 and L8. Leggett et al. (2002a) attribute this behavior to variations in the amount of dust present in the photospheres of these objects. We concur that the scatter (which is larger than our photometric uncertainties) must be intrinsic to the objects themselves. This scatter is also apparent in z^*-J colors, but not in $I-z^*$. Note that one object, the L6.5 2M2244+20, is nearly 0.5 mag redder than all other L dwarfs and appears to be an especially peculiar object. There may also be scatter in the colors of mid- and late-T dwarfs, indicated in the $zJHK$ data in Leggett et al. (2002a) and Burgasser et al. (2002), possibly due to variations in H_2 opacity (Burgasser et al. 2002). The color uncertainties in this paper are generally too large and the sample too small for us to say more about these very cool brown dwarfs.

4.3. Color–Absolute Magnitude Relations

Figure 4 also shows the absolute magnitude M_J plotted against $I-J$ and $J-K$. The M_J versus $I-J$ relation shows a tight sequence for late-M and L dwarfs, aside from a few notable outliers that are marked. The M and L dwarfs lying to the right of the sequence may be unresolved binaries or may be young. The object to the left of the sequence (GD165B) may have an error in the $I-J$ color caused by contamination from its bright companion. A simple formula reproduces this sequence: for 37 dwarfs with spectral type M6.5 through L8 (excluding the four outliers PC0025+04, 2M1328+21, GD165B, and LHS102B),

$$M_J = 21.81 - 8.692(I-J) + 1.697(I-J)^2.$$

This formula is valid for $2.8 < I-J < 4.2$. The rms dispersion is only 0.23 mag from this relation, hardly larger than the observational errors. The dispersion here is slightly smaller than was

observed for M_J versus spectral type in Figure 2; there, a similar fit for 45 objects with spectral type M6.5 through L8 (excluding the two greatest outliers LP944−20 and 2M0850+10) is

$$M_J = 8.38 + 0.341 * ST$$

(where $ST = 7$ for spectral type M7 up to 18 for spectral type L8), with a dispersion of 0.25 mag. For the early-T dwarfs SDSS1254-01 and 2M0559-14, M_J appears to be as bright or brighter than for late-L dwarfs, similar to the behavior seen in Fig. 3. A redistribution of flux from the mid-IR into the J band may help to push the $I - J$ colors of T dwarfs 1–2 magnitudes redder than the L dwarfs (see Sec. 5).

The right panels of Figure 4 show that the scatter in the $J - K$ colors of mid- and late-L stars when plotted against M_J persists, just as the scatter appeared when plotted against spectral type. The scatter in absolute magnitude was noticed before (K00), but was somewhat tentative because of the few L dwarfs with measured distances. Figure 4 shows that there is a trend *in the mean* $J - K$ colors of L dwarfs, but the correlation between $J - K$ and M_J for individual stars is very poor. Because M_J is closely coupled with effective temperature for M and L dwarfs (Sec. 4.7 below), Figure 4 shows that some factor in addition to temperature is dominating the $J - K$ colors for L2-L8 dwarfs. This puzzle is discussed further in Section 5 below.

4.4. Color–Color Relations

Figure 5 plots a selection of color-color diagrams for all of the objects with measured optical and near-infrared photometry. They show the utility of the z^* filter both for classification purposes and for deriving physical parameters. Spectral types and subtypes can be accurately estimated using the combination of Iz^*JK photometry. Even z^*, J, and K alone provide an approximate classification, although the scatter in the colors of mid- to late-L dwarfs makes their classification less accurate without additional colors. (Using z^*JK alone is useful for classifying faint dwarfs with SDSS z^* data plus 2MASS or other JK, but without r^* or i^* data. The same technique should be useful for classifying objects with IJK from DENIS.) The L6.5 dwarf with very red $J - K$ color (2M2244+20) clearly merits further study. A parallax determination for this unusual object will be particularly interesting.

The first panel ($J-K$ vs. $I-z^*$) is similar to one studied by Marley et al. (2002), who showed that $i^* - z^*$ and $J - K$ colors are sensitive to the presence of condensates in the atmospheres of cool dwarfs. Cloud-bearing models with sedimentation provide a qualitative understanding of this diagram. The significant scatter and lack of correlation among L dwarfs suggests that different values of the rainout efficiency parameter (see Ackerman & Marley 2001 for details on this model) might be needed to match the data. For T dwarfs, the models predict that $J - K$ will decrease while $I - z^*$ increases, until a maximum is reached in $I - z^*$ for objects that have cooled to between $-0.5 > J - K > -1.5$ (depending on rainout efficiency parameter). Our data are roughly consistent with these predictions, although the redder $I - z^*$ color of Gl 570D might suggest that

we have not yet reached the turn around point. However, the $I - z^*$ color for Gl 570D is based on two synthesized magnitudes, and it is also possible that the derived color is more uncertain than is estimated here.

4.5. Kinematics

Tangential velocities of stars comprise two of the three components of their space velocities and, as such, should provide some statistical indication of a population's age. Radial velocity measurements have appeared in the literature for a few stars in this paper, and for them space velocities can be determined. However, for most of the sample, only the tangential velocities are available. A discussion of $V_{\rm tan}$ for a few early- to mid-L dwarfs showed the data were consistent with them having ages $\sim$1 Gyr or older (Gizis et al. 2000). A comparison can be made with the tangential velocities in Table 1 with those of the volume-complete sample of M dwarfs (primarily M0 to M5) in the solar neighborhood from Reid et al. (1995) and Hawley et al. (1996). The dM stars have $< V_{\rm tan} > \simeq 44$ km s^{-1} for all absolute magnitude bins from $M_V = 8.5$ to 14.5 (spectral types M0 to M5), and 27% of the stars have $V_{\rm tan} \geq 60$ km s^{-1}. The subset of dMe stars have somewhat smaller motions due to their younger mean age, with $< V_{\rm tan} >= 31$ km s^{-1}. The objects in Table 1 have $< V_{\rm tan} >= 34 \pm 5$ km s^{-1} and four objects (14%) have $V_{\rm tan} \geq 60$ km s^{-1}. These results are intermediate between the values for all dM stars and the dMe stars. Comparison with a relation between age and velocity dispersion for disk stars (e.g. Wielen 1977) indicates that the sample has a mean age of 2-4 Gyr. One star (GRH2208−20) has a moderately-high velocity, suggesting (but not requiring) thick-disk or even halo membership; if it is excluded, the remaining sample has $< V_{\rm tan} >= 31 \pm 4$ km s^{-1} There is no obvious difference between the M, L, and T dwarfs in Table 1.

These results show that the objects in this paper have slightly smaller space motions compared to the earlier-type M dwarfs, although the difference is of marginal significance. A very similar result has been found by Reid et al. (2002) for a large sample of late-M dwarfs (M7 to M9.5). A difference like this could be caused by a Malmquist bias — the preferential discovery of more luminous L and T dwarfs that would be systematically younger and have smaller velocities. However, the small dispersion in absolute magnitudes seen in Figure 4, M_J vs. $I - J$, would indicate that not much dispersion exists among most late-M and L dwarfs to affect the kinematics of the sample. Reid et al. (2002) drew the same conclusion for their late-M dwarfs. Alternatively, smaller space motions for L and T dwarfs compared to M dwarfs can be understood as a result of a combination of two factors. First, late-L and T dwarfs encompass a wider range of masses at a given effective temperature than do M dwarfs, as can be seen from evolutionary models (e.g. Chabrier et al. 2000) over a range of ages. Second, a rising IMF boosts the number of lower-mass and younger objects. This second factor becomes more important if the IMF is steep, but is significant even with a slowly rising IMF (e.g. $\alpha \sim 1$). A simple population model with these factors predicts a drop in space velocities in agreement with the observed values, and predicts a

further drop for T dwarfs as long as the IMF continues to rise for lower masses. The reality of this difference in motions between the M0-M5 dwarfs and cooler dwarfs, and its cause, can be studied further when larger samples of L and T dwarfs are available.

4.6. Stellar Models and Ages

The color-absolute magnitude diagram for M and L dwarfs shown in Figure 4 is repeated in Figure 6, with evolutionary models taken from Chabrier et al. (2000) using DUSTY model atmospheres (Allard et al. 2001) added for comparison with the data. T dwarfs are omitted because the DUSTY models are known to be inappropriate for T dwarfs, where the photospheres are dominated by molecular opacity, not dust. The models with ages consistent with the kinematics of the sample (ages of several Gyr) match the data qualitatively, but significant differences are apparent: for late-M and early-L stars, the models predict optical and near-IR colors bluer than are observed; for late-L dwarfs, the models predict near-IR colors much redder and optical colors slightly redder than are observed. These differences have been noted previously (e.g. Leggett et al. 2000a; Leggett et al. 2001), as have other symptoms of models that are not totally correct for these very challenging cool atmospheres (e.g. Reid & Cruz 2002). The differences have been attributed, at least in part, to incorrect opacity tables for H_2O used in the model atmospheres for late-M dwarfs, and the unrealistic assumption that all dust remains in the atmosphere of late-L dwarfs. Models in which dust is distributed in stratified clouds and is below the photosphere in late-L and T dwarfs (e.g. Marley et al. 2002; Allard et al. in preparation) should provide a much better match to the data. Meanwhile, the empirical fit determined in Sec. 4.3 and plotted in Figure 6 describes the sequence of disk L dwarfs much more accurately than the dusty models.

4.7. Temperatures of Late-M and L Dwarfs

Effective temperatures can be calculated from the absolute magnitudes from this paper if the bolometric corrections and stellar radii can be determined. This method of determining temperatures is potentially very accurate for the low-mass objects in this paper, because only the radii are model-dependent, and the radii depend primarily on the interior models which are relatively well known. Deficiencies in the model atmospheres, such as discussed in the previous section, have little effect on the derived temperatures using this approach. This method was first applied to an L dwarf to estimate the temperature of 2M1523+30 (Gl 584C) by K00, and has been used by others (e.g. Leggett et al. 2001; Leggett et al. 2002a; Burgasser et al. 2002). Here we repeat the procedure for the late-M and L dwarfs in this paper with known distances.

Bolometric corrections for K-band (BC_K) have been calculated by Leggett et al. (2001), Leggett et al. (2002a) and references therein for M and L dwarfs. Values for BC_J have been calculated by Reid et al. (2001a), and they agree very well for M through mid-L dwarfs,

but are up to 0.4 mag different for L7.5-L8 dwarfs. The difference comes from Leggett's use of L-band photometry and assuming a Rayleigh-Jeans flux distribution at longer wavelengths, thus deriving a larger luminosity and smaller values for BC_K and BC_J than the values derived by Reid et al. The different results point out our uncertainty in the flux emitted longward of 3 microns by these very cool objects. Nevertheless, because the temperature depends on the fourth root of the luminosity, temperatures can still be derived despite this uncertainty. An interpolation formula for BC_K vs. $I - K$ was derived by Leggett et al. for M and L dwarfs, and is adopted here. (A formula for BC_K vs. $J - K$ was also derived, but is not as well established for late-L dwarfs, with their wide range of $J - K$ colors, so is not used here.) This formula predicts values for BC that are 0.1 mag larger than calculated by Leggett et al. (2002a) and 0.3 mag smaller than calculated by Reid et al. (2001a) for L7.5-L8 dwarfs.

Stellar radii for models from the Lyon group (Chabrier et al. 2000) and from the Arizona group (Burrows et al. 1997) have a small systematic difference throughout the regime of intermediate-age and old L dwarfs: the models from the Lyon group have radii consistently larger by 6% at a given age and luminosity than those from the Arizona group. Here we adopt an interpolation formula

$$R/R_\odot = 0.088 + 0.00070(16.2 - M_{\rm bol})^{2.9}$$

that predicts radii half way between the 1 Gyr and 5 Gyr models from the two groups over the range 12-16.5 in $M_{\rm bol}$. Therefore, the temperatures derived here would be higher if one were to adopt radii from the Arizona models, and lower if one were to adopt radii from the Lyon models, but the differences would be only 40 K for M dwarfs and 20 K for late-L dwarfs. We estimate an error in BC_K of ± 0.05 mag at $M_{\rm bol} = 12$ increasing to ± 0.10 mag at $M_{\rm bol} = 16$, and an error in $R/R_\odot$ of $\pm$3-6% at $M_{\rm bol}$ = 12-16.

Table 5 contains the derived effective temperatures for the M and L dwarfs in Tables 1 and 3 with the requisite data (parallax and $I_C JK$ photometry). Selected relations based on these temperatures are presented in Figure 7. Use of bolometric corrections from Reid et al. (2001a) would result in temperatures cooler by 100 K for the coolest three stars. For other objects, the estimated BC_K could have a systematic error, but plausible systematic errors are included in the error bars and can be seen to be quite small. The temperatures derived here are hotter for late-M and early-L dwarfs and cooler for late-L dwarfs than those derived in some other studies (Basri et al. 2000; Leggett et al. 2001; Schweitzer et al. 2001; Schweitzer et al. 2002; Chabrier 2002) using fitting of model atmospheres to spectroscopic data. These differences are probably further manifestations of the imperfect models used in those studies, discussed in the previous section. The mean temperature derived here for the three latest L dwarfs (L7.5-L8) is 1360 K. The relation between $T_{\rm eff}$ and spectral type for L dwarfs shown in the bottom panel of Figure 7 is very similar to the relation derived by Stephens et al. (2001) using $K - L$ colors and the models of Marley et al. (2002).

The scatter in the bottom panel of Figure 7 is larger than might be expected, given the tight relations between M_J, $I - J$, and spectral type seen in Figure 4. (The range of M_J at a

given spectral type seen in Figure 2 is another symptom of the scatter in Figure 7.) Some objects (e.g., T513−46546, LP944−20, 2M0850+10) are cooler than the mean for their spectral type, whereas others (Kelu-1, 2M1112+35, DEN0205−11) are warmer. The range in temperature of 200-300 K at a given spectral type is somewhat larger than might be expected from the formal errors. Unresolved binaries (in addition to the binaries already noted in the tables and accounted for in Figure 7) will contribute to this scatter, because they will have measured luminosities too large (by up to a factor of two), adopted radii too large (by up to 10% for late-M dwarfs, less for L dwarfs), and derived temperatures too hot by up to 240 K. However, the small scatter in Figure 4 makes it unlikely that many of the objects are unresolved binaries, enough to account for the range of temperatures seen in the bottom panel of Figure 7. Furthermore, a few objects may be significantly younger (ages $\leq 10^8$ yr), have radii larger than assumed, and their derived temperatures will be too high. Much of the observed scatter could be accounted for by revisions in the spectral types assigned to a few stars. This possibility would require changing the type of T513−46546 to a later type of L0 (instead of M8.5), LP944−20 to L2 (not M9), and 2M0850+10 to L7-L8 (not L6); and if they are not binary (triple or greater, in the case of DEN0205−11!) or young, revising Kelu-1 to an earlier type of L0-L1 (not L2), 2M1112+35 L3 (not L4.5), and DEN0205−11 L6 (not L7). Such revisions in spectral type would be completely inconsistent with the morphology of the optical spectra for at least some of these well-studied objects. Using spectral types from Martín et al. (1999c) or Geballe et al. (2002) would not reduce the observed scatter in this diagram. Alternatively, spectral types may be affected to a relatively minor extent by some other physical parameter(s) in addition to temperature, thus leading to an imperfect correlation with temperature that is seen in Figure 7.

5. CONCLUSIONS

New or improved parallax measurements have been presented for 28 late-type dwarfs, including 17 L and 3 T dwarfs. Optical ($VRIz^*$) and near-IR (JHK) photometry is also presented for these and other cool dwarfs. Various colors are used to explore spectral type vs. color vs. magnitude diagrams. Enough L dwarfs are included to begin to define their absolute magnitudes reasonably well, but a larger sample of T dwarfs is needed. The $I - J$ color is a good predictor of absolute magnitude for late-M and L dwarfs, spectral type is almost as good, but JHK colors are notably inferior for predicting absolute magnitude.

While only one L/T transition object has a measured parallax, it and one of the mid-T dwarfs both show M_J brighter than for the latest L dwarfs. This brightening of M_J is accompanied by an increase in $I - J$ and a decrease in $J - K$, all indicative of an increase in the fraction of total flux emitted in the J band for early-T dwarfs compared to late-L dwarfs, but with little difference in luminosity. Apparently the early-T dwarfs have less dust above the photosphere, or perhaps holes have developed through high-level dust clouds, leading to increased molecular absorption at mid-IR wavelengths, a redistribution of flux into the J band, and the observed changes in colors.

This brightening for early-T dwarfs would then be a temporary phenomenon following the dusty L-dwarf phase and prior to cooling further to late-T spectral type. This picture is consistent with the precipitation condensates described by Ackerman & Marley (2001), for example. If confirmed with a larger sample, this behavior will affect the space density derived for these objects.

The combination of z^*JK colors alone can be used to accurately classify late-M, early-L, and T dwarfs, and predict their absolute magnitudes, but is less effective at untangling the scatter among mid- and late-L dwarfs. The tangential velocity is derived for each object, and the mean velocity is slightly less than that for dM stars in the solar neighborhood, consistent with a sample with a mean age of several Gyr. Using colors to estimate bolometric corrections, and models to estimate stellar radii, effective temperatures are derived for the late-M and L dwarfs with known distances. The latest L dwarfs are found to have $T_{\rm eff} \sim 1360$ K, with a range of 1250-1400 K allowed by uncertainties in the bolometric corrections.

The $J-K$ colors of L dwarfs are thought to be affected by the distribution of dust in the atmosphere. Objects with dust distributed high in the atmosphere should have redder $J-K$ colors, more in agreement with the DUSTY models described in Figure 6. In contrast, objects with atmospheres partially clear of dust (perhaps because sedimentation or precipitation dominates over turbulent mixing in the upper atmosphere) should have stronger molecular absorption and $J-K$ colors that are not as red. This behavior is shown in the models of Marley et al. (2002) as their rainout parameter is changed. This picture seems plausible, but it is not yet clear what underlying physical parameters cause the different behavior among objects that otherwise appear similar. A factor that could be important is rotation velocity. The nine L dwarfs that have measurements of $v\sin i$ (Basri et al. 2000; Reid et al. 2002) all show a significant rotation, but there is not an obvious correlation between the measured $v\sin i$ and the $J-K$ color. For example, Kelu-1 and DEN1058-15 both have fast rotation, but Kelu-1 is redder than the mean for its absolute magnitude, while DEN1058-15 is bluer. Kelu-1 may be atypical for a field L dwarf, and its high rotation velocity and/or its red $J-K$ color may be related to its variability (Clarke et al. 2002). Measurements of $v\sin i$ for additional L dwarfs may help reveal whether a correlation exists. Of course, the distribution of dust could be quite sensitive to small effects, and more than one factor could be contributing to the scatter seen in L dwarfs so as to mask any simple correlation. Parameters such as metallicity and magnetic field strength come to mind as plausible factors to affect the dust content of these objects. We consider the puzzling behavior of the near-IR flux of L dwarfs to be an important problem for understanding these objects.

Parallax measurements for additional cool dwarfs are desirable, especially for T dwarfs, for further understanding of their properties. The faintness at optical wavelengths of late-L and T dwarfs precludes observing substantial numbers of them with moderate-size telescopes and CCD cameras. The astrometric satellites being planned, even those like GAIA and SIM that are designed to observe faint targets, are unlikely to help for the same reason. We will continue the present CCD parallax work and may include some of the brightest objects as they are discovered, but observing many objects this way is very time consuming. Further progress will require larger

telescopes and/or observing at near-IR wavelengths where the targets are brighter. The USNO IR group has commissioned a camera employing an ALADDIN InSb array on the Strand 1.55 m telescope, and is now one year into an exploratory program of measuring parallaxes with J and H filters. This program currently includes 13 L dwarfs with spectral type L6 or later and 16 T dwarfs, in addition to the three T dwarfs in Table 1. Results from this program should be a first step in providing the substantial numbers of late-L and T dwarfs with parallax measurements that are needed.

We thank the referee, Sandy Leggett, for a careful reading of the manuscript and for several useful suggestions for clarifying the presentation. We thank our colleagues in SDSS for alerting us to their discovery of the two T dwarfs prior to publication. We thank the WIYN Queue staff for taking photometric data of some of these objects with the WIYN telescope. This publication makes use of data products from the Two Micron All Sky Survey, which is a joint project of the University of Massachusetts and the Infrared Processing and Analysis Center/California Institute of Technology, funded by the National Aeronautics and Space Administration and the National Science Foundation. This research has made use of the Simbad database, operated at CDS, Strasbourg, France.

6. APPENDIX

Column 1 of Table A1 gives the full names of the stars listed in Tables 1, 2, and 3 in the main body of this paper. Additional data for each object is given as extracted from the literature: the second and third columns give the approximate J2000.0 coordinates, the fourth column gives a reference for the coordinates, and the fifth column gives a reference where an identification chart can be found.

REFERENCES

Ackerman, A., & Marley, M. 2001, ApJ, 556, 872

Allard, F., Hauschildt, P.H., Alexander, D.R., Tamanai, A., & Schweitzer, A. 2001, ApJ, 556, 357

Bailer-Jones, C.A.L., & Mundt, R. 2001, A&A, 367, 218

Basri, G. 2000, ARA& A, 38, 485

Basri, G., Mohanty, S., Allard, F., Hauschildt, P.H., Delfosse, X., Martín, E.L., Forveille, T., & Goldman, B. 2000, ApJ, 538, 363

Becklin, E.E., & Zuckerman, B. 1988, Nature, 336, 656

Bessell, M.S. 1990a, PASP, 102, 1181

Bessell, M.S. 1990b, A&AS, 83, 357

Burgasser, A.J. 2001, Ph.D. Dissertation, California Institute of Technology

Burgasser, A.J., et al. 1999, ApJ, 522, L65

Burgasser, A.J., et al. 2000a, AJ, 120, 1100

Burgasser, A.J., et al. 2000b, ApJ, 531, L57

Burgasser, A.J., et al. 2000c, in From Giant Planets to Cool Stars, ASP Conf. Ser. 212, ed. C.A. Griffith & M.S. Marley (San Francisco: ASP), 65

Burgasser, A.J., et al. 2002, ApJ, 564, 421

Burrows, A., & Sharp, C.M. 1999, ApJ, 512, 843

Burrows, A., Hubbard, W.B., Lunine, J.I., & Liebert, J. 2001, Rev. Mod. Phys., 73, 719

Burrows, A., Burgasser, A.J., Kirkpatrick, J.D., Liebert, J., Milsom, J.A., Sudarsky, M.D., & Hubeny, I. 2002, ApJ, in press, astro-ph/0109227

Burrows, A., Marley, M., Hubbard, W.B., Lunine, J.I., Guillot, T., Saumon, D., Freedman, R., Sudarsky, D., & Sharp, C. 1997, ApJ, 491, 856

Carpenter, J.M. 2001, AJ, 121, 2851

Chabrier, G. 2002, ApJ, in press, astro-ph/0110024

Chabrier, G., & Baraffe, I. 2000, ARA&A, 38, 337

Chabrier, G., Baraffe, I., Allard, F., & Hauschildt, P. 2000, ApJ, 542, 464

Clarke, F.J., Tinney, C.G., & Covey, K.R. 2002, MNRAS, in press, astro-ph/0201162

Dahn, C.C., et al. 2000, in From Giant Planets to Cool Stars, ASP Conf. Ser. 212, ed. C.A. Griffith & M.S. Marley (San Francisco: ASP), 74

Delfosse, X., et al. 1997, A&A, 327, L25

Elias, J.H., Frogel, J.A., Matthews, K., & Neugebauer, G. 1982, AJ, 87, 1029

Epchtein, N., et al. 1997, The Messenger, No. 87, 27

Fan, X., et al. 2000, AJ, 119, 928

Forrest, W.J., Skrutskie, M.F., & Shure, M. 1988, ApJ, 330, L119

Geballe, T.R., Kulkarni, S.R., Woodward, C.E., & Sloan, C.G. 1996, ApJ, 467, L101

Geballe, T.R., Saumon, D., Leggett, S.K., Knapp, G.R., Marley, M.S., & Lodders, K. 2001, ApJ, 556, 373

Geballe, T.R., et al. 2002, ApJ, 564, 466

Giclas, H. et al. 1964, Lowell Obs. Bull., No. 124, v. VI, No. 5

Gilmore, G., Reid, N., & Hewett, P. 1985, MNRAS, 213, 257

Gizis, J.E., Monet, D.G., Reid, I.N., Kirkpatrick, J.D., Liebert, J., & Williams, R.J. 2000, AJ, 120, 1085

Gizis, J.E., Kirkpatrick, J.D., & Wilson, J.C. 2001, AJ, 121, 2185

Goldman, B., et al. 1999, A&A, 351, L5

Golimowski, D.A., Burrows, C.J., Kulkarni, S.R., Oppenheimer, B.R., & Brukardt, B. 1998, AJ, 115, 2579

Hauschildt, P.H., Starrfield, S., Allard, F., & Alexander, D.R. 1997, ARA&A, 35, 137

Hawley, S.L., Gizis, J.E., & Reid, I.N. 1996, AJ, 112, 2799

The Hipparcos and Tycho Catalogues 1997, (Noordwijk: ESA)

Irwin, M., McMahon, R.G., & Reid, N. 1991, MNRAS, 252, 61p

Kirkpatrick, J.D. 1998, in ASP Conf. Ser. 134, Brown Dwarfs and Extrasolar Planets, ed. R. Rebolo, E.L. Martín, & M.R. Zapatero Osorio (San Francisco: ASP), 405

Kirkpatrick, J.D., Beichman, C.A., & Skrutskie, M.F. 1997a, ApJ, 476, 311

Kirkpatrick, J.D., Henry, T.J., & Irwin, M.J. 1997b, AJ, 113, 1421

Kirkpatrick, J.D., Henry, T.J., & Liebert, J. 1993, ApJ, 406, 701

Kirkpatrick, J.D., Henry, T.J., & McCarthy, D.W. 1991, ApJS, 77, 417

Kirkpatrick, J.D., Henry, T.J., & Simons, D.A. 1995, AJ, 109, 797

Kirkpatrick, J.D., et al. 1999, ApJ, 519, 802 (K99)

Kirkpatrick, J.D., et al. 2000, AJ, 120, 447 (K00)

Kirkpatrick, J.D., Dahn, C.C., Monet, D.G., Reid, I.N., Gizis, J.E., Liebert, J., & Burgasser, A.J. 2001, AJ, 121, 3235

Koerner, D.W., Kirkpatrick, J.D., McElwain, M.W., & Bonaventura, N.R. 1999, ApJ, 526, L25

Landolt, A.U. 1983, AJ, 88, 439

Landolt, A.U. 1992, AJ, 104, 340

Lane, B.F., Zapatero Osorio, M.R., Britton, M.C., Martín, E.L., & Kulkarni, S.R. 2001, ApJ, 560, 390

Leggett, S.K. 1992, ApJS, 82, 351

Leggett, S.K., Allard, F., Dahn, C., Hauschildt, P.H., Kerr, T.H., & Rayner, J. 2000a, ApJ, 535, 965

Leggett, S.K., Allard, F., Geballe, T.R., Hauschildt, P.H., & Schweitzer, A. 2001, ApJ, 548, 908

Leggett, S.K., Allard, F., & Hauschildt, P.H. 1998, ApJ, 509, 836

Leggett, S.K., Toomey, D.W., Geballe, T.R., & Brown, R.H. 1999, ApJ, 517, L139

Leggett, S.K., et al. 2000b, ApJ, 536, L35

Leggett, S.K., et al. 2002a, ApJ, 564, 452

Leggett, S.K., Hauschildt, P.H., Allard, F., Geballe, T.R., & Baron, E. 2002b, MNRAS, in press, astro-ph/0112335

Liebert, J. 2000, in From Giant Planets to Cool Stars, ASP Conf. Ser. 212, ed. C.A. Griffith & M.S. Marley (San Francisco: ASP), 7

Liebert, J., Kirkpatrick, J.D., Reid, I.N., & Fisher, M.D. 1999, ApJ, 519, 345

Luyten, W.J. 1979a, NLTT Catalogue, Vol. II (Minneapolis: Univ. of Minnesota)

Luyten, W.J. 1979b, LHS Catalogue, 2nd Ed. (Minneapolis: Univ. of Minnesota)

Luyten, W.J. & Albers, H. 1979, LHS Atlas (Minneapolis: Univ. of Minnesota)

Marley, M.S., Seager, S., Saumon, D., Lodders, K., Ackerman, A.S., Freedman, R.S., & Fan, X. 2002, ApJ, 568, 335

Martín, E.L., Basri, G., Delfosse, X., & Forveille, T. 1997, A&A, 327, L29

Martín, E.L., Basri, G., & Zapatero Osorio, M.R. 1999a, AJ, 118, 1005

Martín, E.L., Brandner, W., & Basri, G. 1999b, Science, 283, 1718

Martín, E.L., Delfosse, X., Basri, G., Goldman, B., Forveille, T., & Zapatero Osorio, M.R. 1999c, AJ, 118, 2466

Martín, E.L., Zapatero Osorio, M.R., & Lehto, H.J. 2001, ApJ, 557, 822

McLean, I.S., Prato, L, Kim, S.S., Wilcox, M.K., Kirkpatrick, J.D., & Burgasser, A. 2002, ApJ, 561, L115

Monet, D.G., Dahn, C.C., Vrba, F.J., Harris, H.C., Pier, J.R., Luginbuhl, C.B., & Ables, H.D. 1992, AJ, 103, 638

Nakajima, T., Oppenheimer, B.R., Kulkarni, S.R., Golimowski, D.A., Matthews, K., & Durrance, S.T. 1995, Nature, 378, 463

Oppenheimer, B.R., Kulkarni, S.R., Matthews, K., & Nakajima, T. 1995, Science, 270, 1478

Oppenheimer, B.R., Kulkarni, S.R., Matthews, K., & van Kerkwijk, M.H. 1998, ApJ, 502, 932

Pavlenko, Y., Zapatero Osorio, M.R., & Rebolo, R. 2000, A&A, 355, 245

Pier, J.R., et al. 2000, in From Giant Planets to Cool Stars, ASP Conf. Ser. 212, ed. C.A. Griffith & M.S. Marley (San Francisco: ASP), 30

Potter, D., Martín, E.L., Cushing, M.C., Baudoz, P., Brandner, W., Guyon, O., & Neuhäuser, R. 2002, ApJ, in press, astro-ph/0201431

Reid, I.N., et al. 1999, ApJ, 521, 613

Reid, I.N., Burgasser, A.J., Cruz, K.L., Kirkpatrick, J.D., & Gizis, J.E. 2001a, AJ, 121, 1710

Reid, I.N., Gizis, J.E., Kirkpatrick, J.D., & Koerner, D.W. 2001b, AJ, 121, 489

Reid, I.N., & Hawley, S.L. 2000, New Light on Dark Stars (Chichester: Praxis)

Reid, I.N., Hawley, S.L., & Gizis, J.E. 1995, AJ, 110, 1838

Reid, I.N., & Cruz, K.L. 2002, AJ, 123, 466

Reid, I.N., Kirkpatrick, J.D., Liebert, J., Gizis, J.E., Dahn, C.C. & Monet, D.G. 2002, AJ, in press, astro-ph/0204285

Ruiz, M.T., Leggett, S.K., & Allard, F. 1997, ApJ, 491, L107

Schneider, D.P., Greenstein, J.L., Schmidt, M., & Gunn, J.E. 1991, AJ, 102, 1180

Schneider, D.P., et al. 2002, AJ, 123, 458

Schweitzer, A., Gizis, J.E., Hauschildt, P.H., Allard, F., Howard, E.M., & Kirkpatrick, J.D. 2002, ApJ, 566, 435

Schweitzer, A., Gizis, J.E., Hauschildt, P.H., Allard, F., & Reid, I.N. 2001, ApJ, 555, 368

Skrutskie, M.F., et al. 1997, in The Impact of Large-Scale Near-IR Sky Surveys, ed. F. Garzon et al. (Dordrecht: Kluwer), 25

Smith, J.A., et al. 2002, AJ, in press, astro-ph/0201143

Steele, I.A., & Howells, L. 2000, MNRAS, 313, L43

Stephens, D.C., Marley, M.S., Noll, K.S., & Chanover, N. 2001, ApJ, 556, L101

Strauss, M.A., et al. 1999, ApJ, 522, L61

Testi, L., et al. 2001, ApJ, 552, L147

Tinney, C.G. 1996, MNRAS, 281, 644

Tinney, C.G., & Tolley, A.J. 1999, MNRAS, 304, 119

Tinney, C.G., Mould, J.R., & Reid, I.N. 1993, AJ, 105, 1045

Tinney, C.G., Reid, I.N., Gizis, J., & Mould, J.R. 1995, AJ, 110, 3014

Tinney, C.G., Delfosse, X., Forveille, T., & Allard, F. 1998, A&A, 338, 1066

Tokunaga, A.T., Simons, D.A., & Vacca, W.D. 2002, PASP, 114, 180

Tsvetanov, Z.I., et al. 2000, ApJ, 531, L61

van Altena, W.F., Lee, J.T., & Hoffleit, E.D. 1995, The General Catalogue of Trigonometric Stellar Parallaxes, Fourth Edition (Schenectady: L. Davis Press)

Wielen, R. 1977, A&A, 60, 263

Wilson, J.C., Kirkpatrick, J.D., Gizis, J.E., Skrutskie, M.F., Monet, D.G., & Houck, J.R. 2001, AJ, 122, 1989

York, D.G., et al. 2000, AJ, 120, 1579

Fig. 1.— Differences between JHK magnitudes of late-M and L dwarfs observed in the CIT system (data in Table 2 of this paper) and in the 2MASS system (left panels, data from various sources) and in the MKO system (right panels, data from Table 3 of Leggett et al. 2001b). T dwarfs will behave differently, and are not included.

Fig. 2.— Absolute magnitudes of cool dwarfs with known distances plotted against spectral type. In this and following plots, M dwarfs are plotted with squares, L dwarfs are plotted with circles, and T dwarfs are plotted with triangles.

Fig. 3.— Selected colors of cool dwarfs plotted against spectral type. Squares, circles, and triangles are M, L, and T dwarfs, respectively.

Fig. 4.— Absolute J magnitudes and spectral types of cool dwarfs plotted against $I-J$ and $J-K$ colors. Squares, circles, and triangles are M, L, and T dwarfs, respectively.

Fig. 5.— Selected color—color diagrams of cool dwarfs showing the utility of the z^* filter. Squares, circles, and triangles are M, L, and T dwarfs, respectively.

Fig. 6.— M and L dwarfs compared to the AMES DUSTY models (Chabrier et al. 2000) for three different ages. The solid line shows a fit to the observed M6.5-L8 dwarfs (Sec. 4.3). Squares and circles are M and L dwarfs, respectively.

Fig. 7.— Effective temperatures of M and L dwarfs calculated from M_J (this paper), BC_K (Leggett et al. 2001a), and $R/R_\odot$ (models from Burrows et al. 1997 and Chabrier et al. 2000). Squares and circles are M and L dwarfs, respectively.

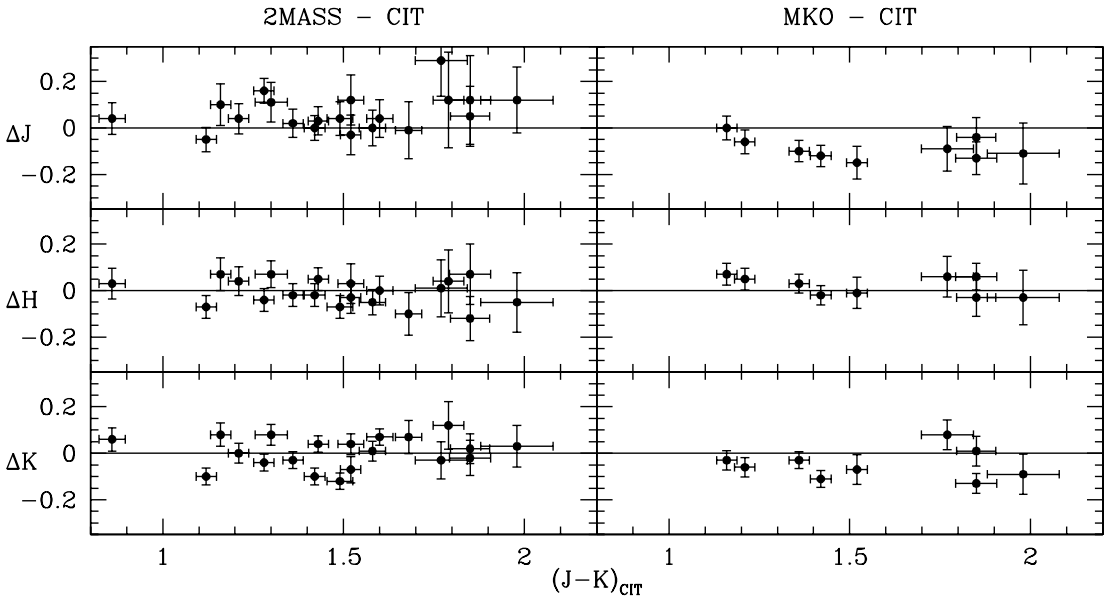
2MASS − CIT
MKO − CIT
ΔJ
ΔH
ΔK
0.2
0
−0.2
1
1.5
2
(J−K)CIT

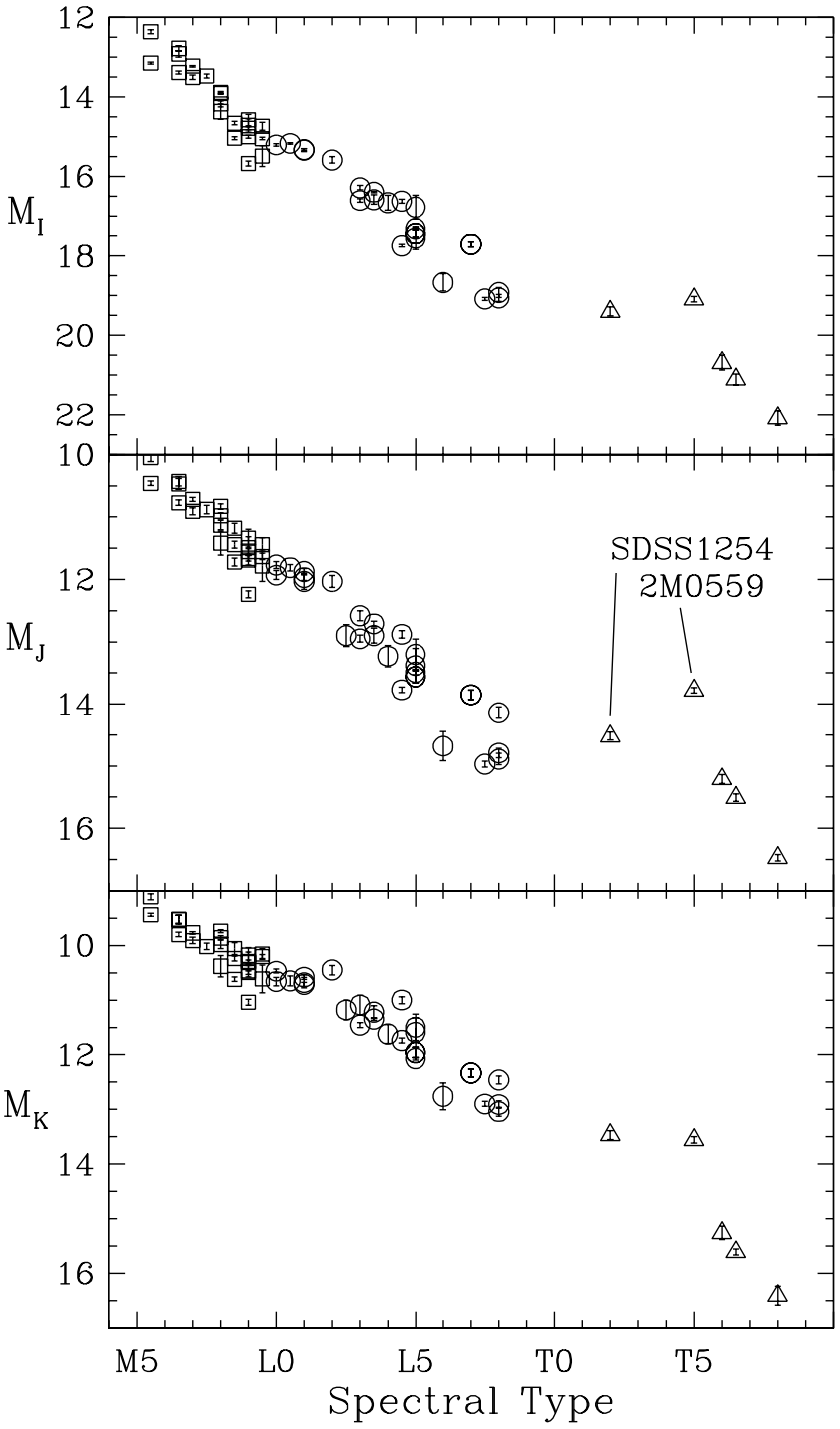
M_I
M_J
M_K
SDSS1254
2M0559
M5
L0
L5
T0
T5
Spectral Type

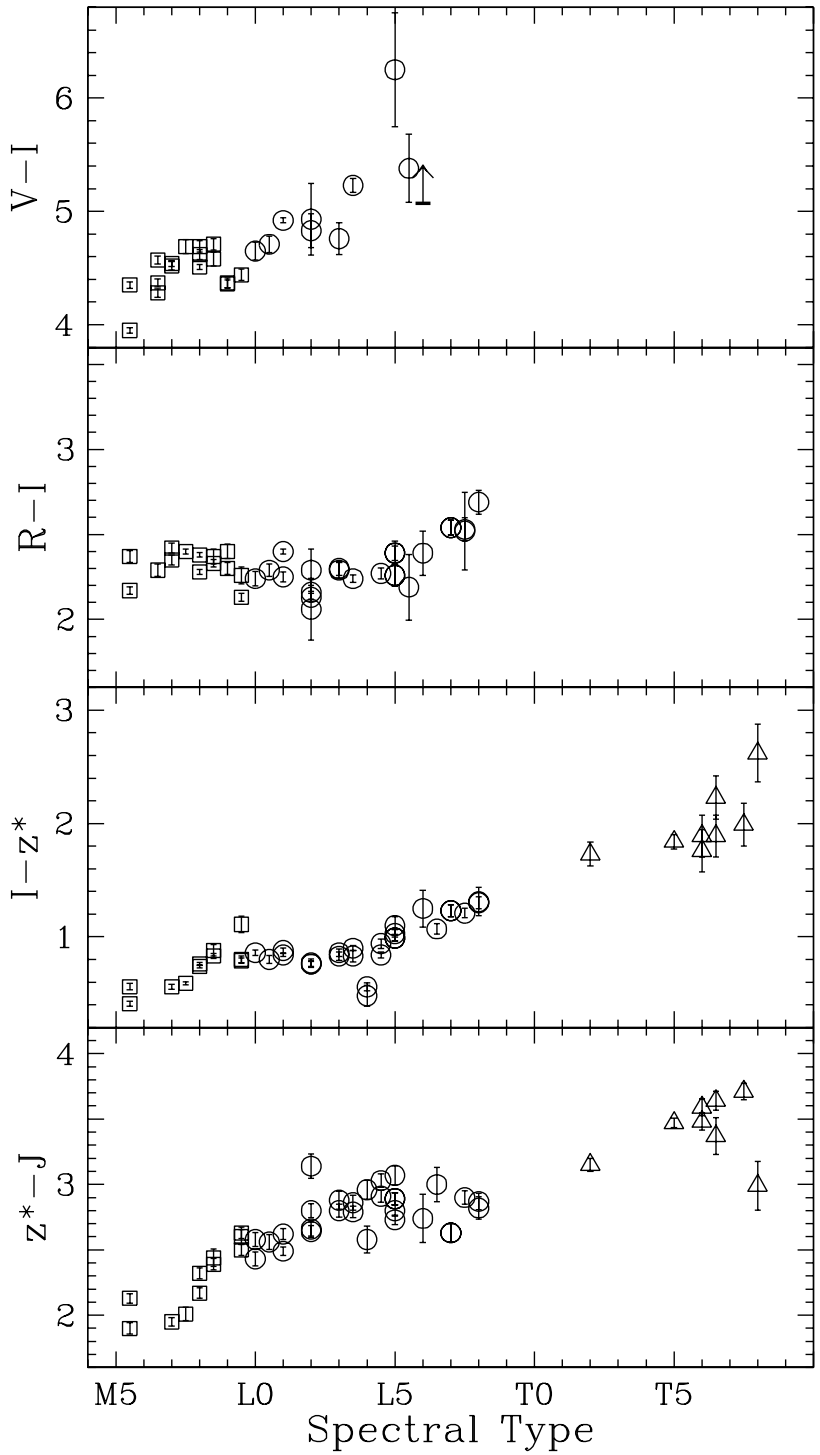
V−I
R−I
I−z*
z*−J
M5
L0
L5
T0
T5
Spectral Type

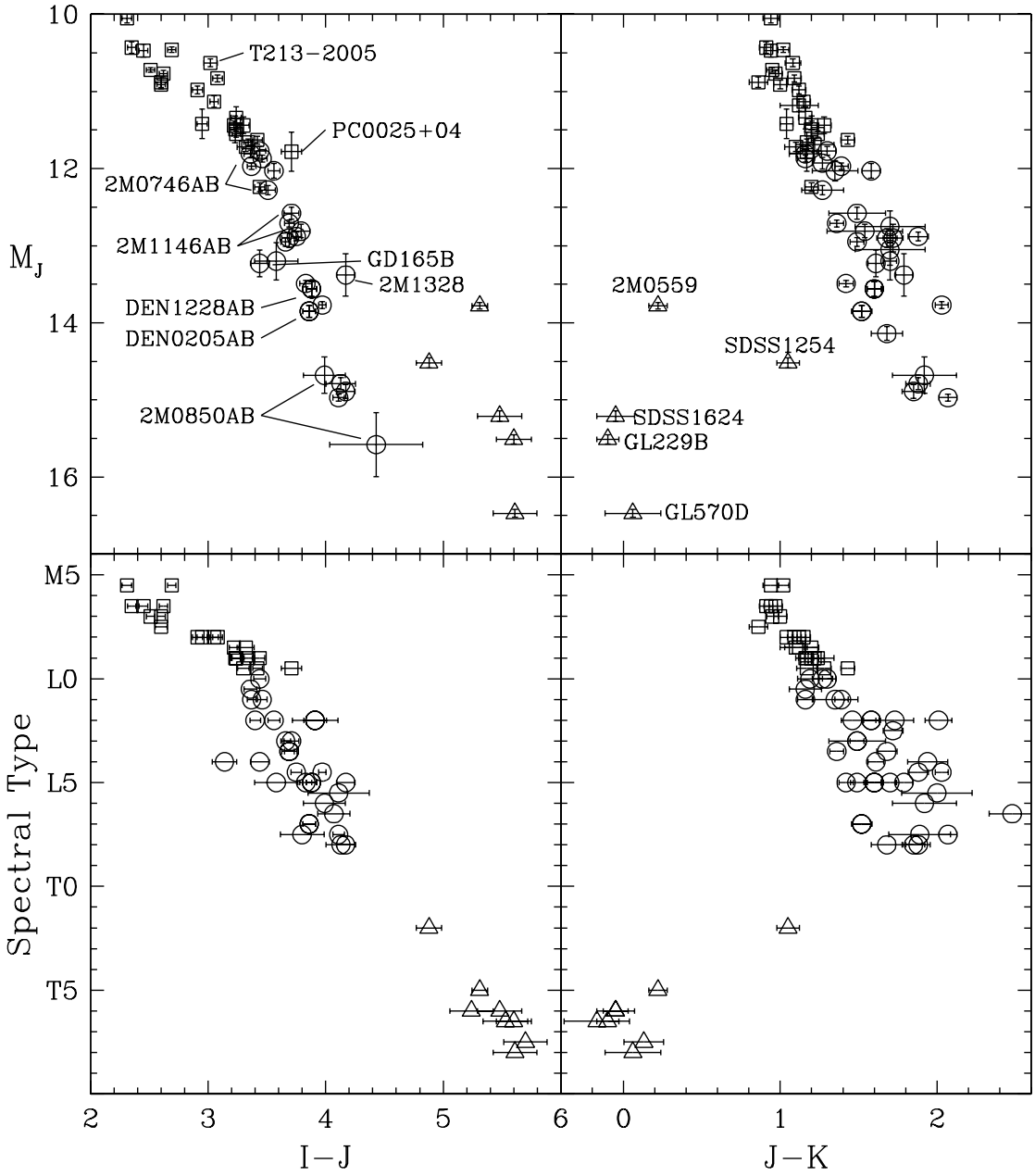
T213−2005
PC0025+04
2M0746AB
2M1146AB
GD165B
2M1328
DEN1228AB
DEN0205AB
2M0850AB
2M0559
SDSS1254
SDSS1624
GL229B
GL570D
M_J
Spectral Type
I−J
J−K
10
12
14
16
M5
L0
L5
T0
T5
2
3
4
5
6
0
1
2

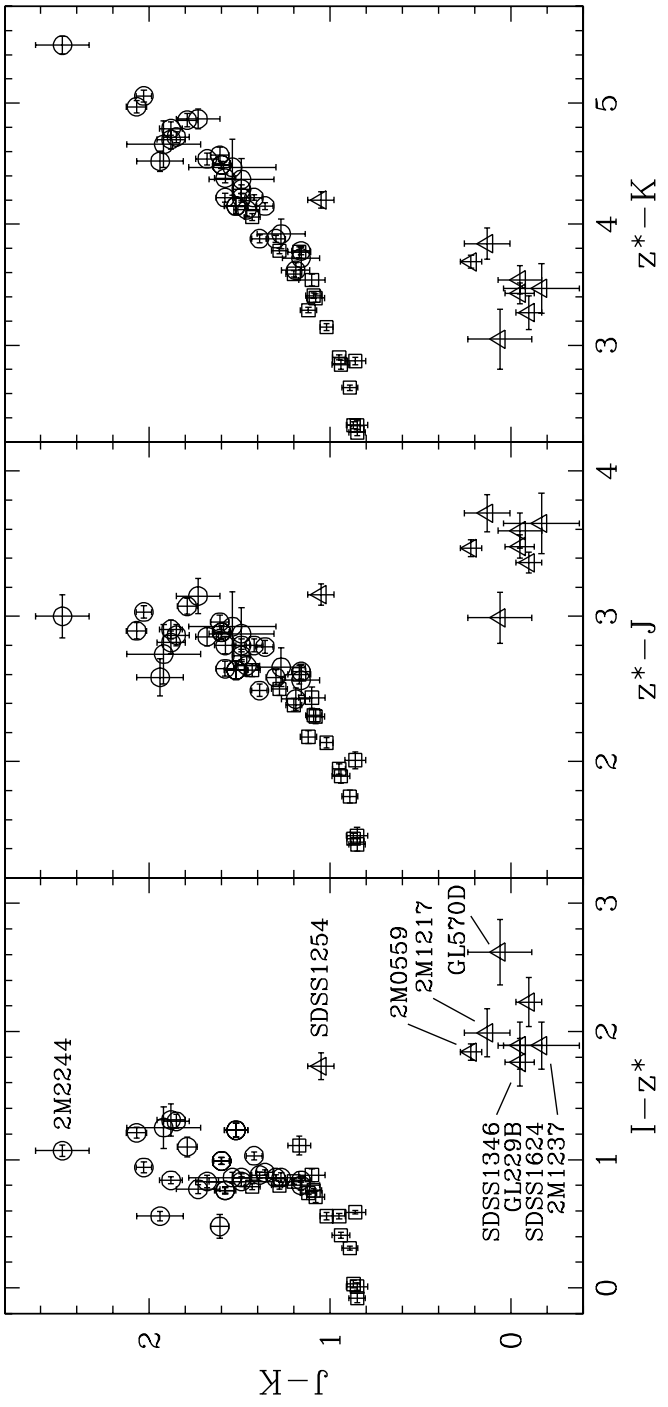
J−K
I−z*
z*−J
z*−K
2M2244
SDSS1254
2M0559
2M1217
GL570D
SDSS1346
GL229B
SDSS1624
2M1237

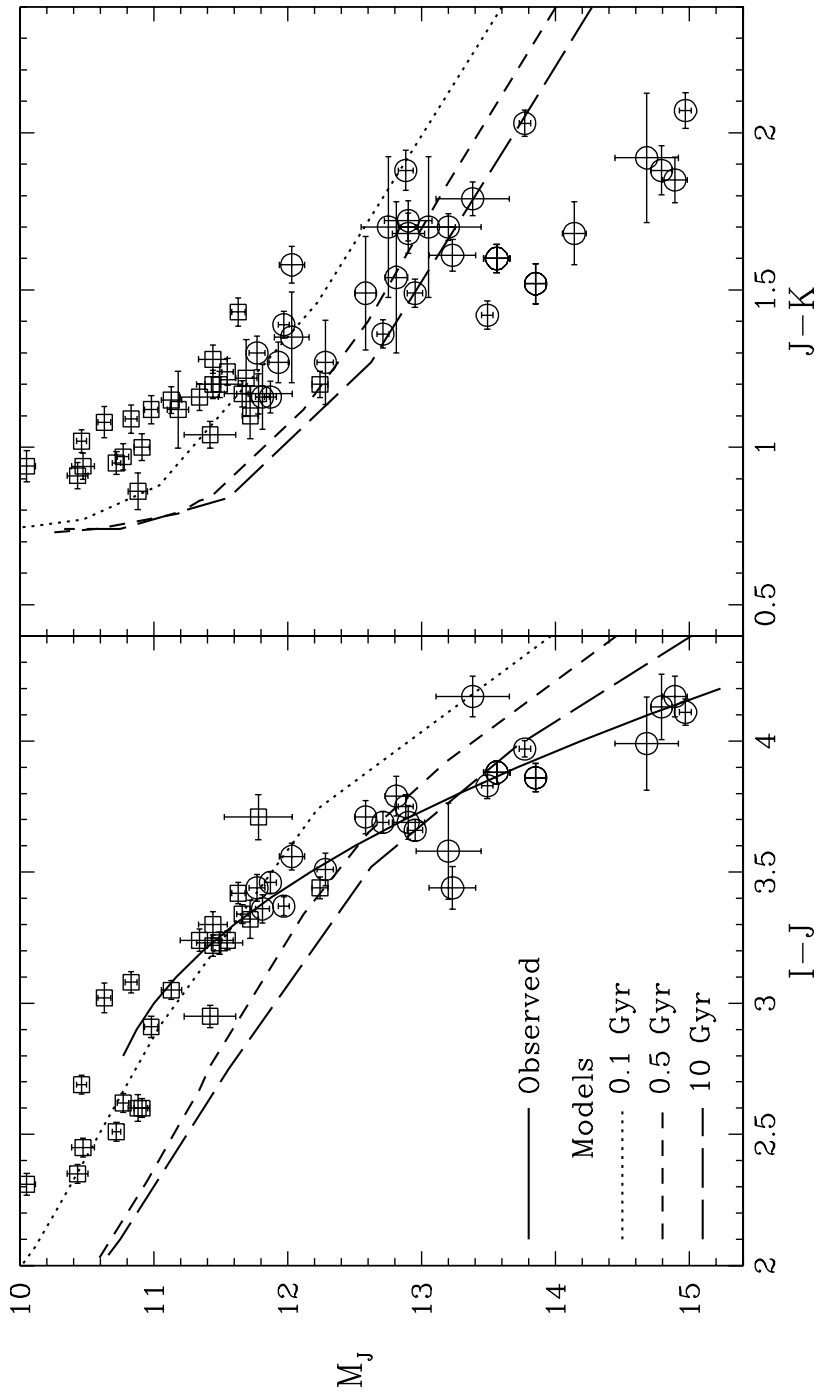
M_J
I−J
J−K
Observed
Models
0.1 Gyr
0.5 Gyr
10 Gyr

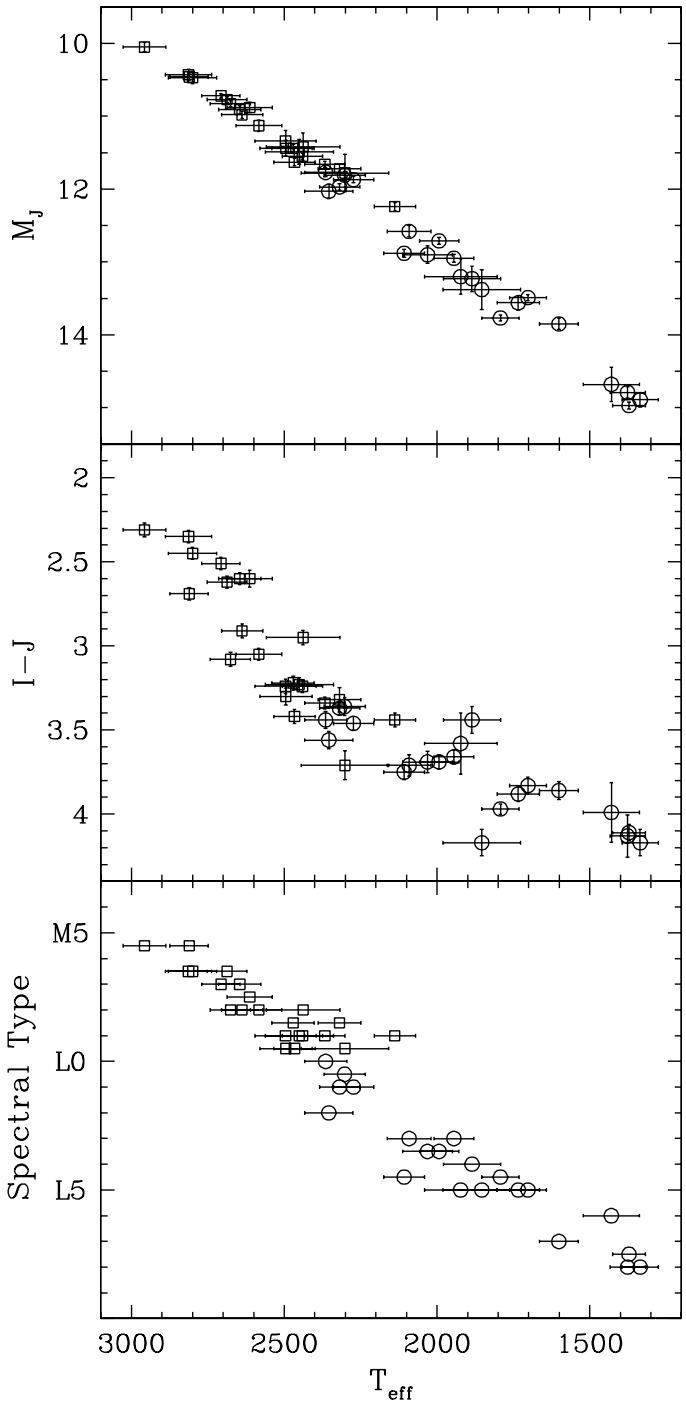
10
12
14
M_J
2
2.5
3
3.5
4
I−J
M5
L0
L5
Spectral Type
3000
2500
2000
1500
T_{eff}

TABLE 1
ASTROMETRY OF LATE-TYPE DWARFS/BROWN-DWARFS

Object Sp. Type	No. Obs. ΔT(yr)	π(rel) (mas)	π(abs) (mas)	μ(rel) (mas yr^{-1})	P.A. (degrees)	$V_{\tan}$ (km s^{-1})
PC0025+04	89	13.2	13.8	10.5	94.6	3.6
M9.5Ve	9.1	1.6	1.6	0.4	1.8	0.4
2M0036+18	59	113.3	114.2	907.1	82.4	37.7
L3.5V	2.9	0.8	0.8	0.6	0.1	0.3
CTI0126+28	92	29.7	30.5	189.6	224.7	29.5
M8.5V	5.3	0.4	0.5	0.2	0.1	0.5
2M0149+29	43	44.0	44.4	438.8	156.4	46.8
M9.5Ve	3.0	0.7	0.7	0.7	0.1	0.7
DEN0205−11[a]	47	49.8	50.6	437.8	82.8	41.0
L7V	3.9	1.5	1.5	0.8	0.1	1.2
T832-10443	89	35.2	36.0	203.3	239.5	26.8
M8V	7.1	0.4	0.4	0.1	0.1	0.3
LP412−31	104	68.3	68.9	432.9	126.2	29.8
M8V	5.0	0.6	0.6	0.3	0.1	0.3
2M0326+29	33	30.1	31.0	69.4	344.3	10.6
L3.5V	3.2	1.5	1.5	0.8	0.7	0.5
2M0345+25	116	36.3	37.1	102.4	249.6	13.1
L0V	4.3	0.5	0.5	0.3	0.2	0.2
2M0559−14	59	96.9	97.7	661.2	121.6	32.1
T5V	2.1	1.2	1.3	1.2	0.1	0.4
2M0746+20[b]	78	81.1	81.9	378.5	261.2	21.9
L0.5V	2.2	0.3	0.3	0.3	0.1	0.1
2M0825+21	27	93.0	93.8	585.6	240.5	29.6
L7.5V	2.0	1.0	1.0	1.4	0.2	0.3
2M0850+10[c]	30	38.4	39.1	144.7	267.0	17.5
L6V	3.3	3.5	3.5	2.0	0.9	1.6
T213-2005	87	29.3	30.1	389.0	277.6	61.3
M:V	7.0	0.4	0.4	0.1	0.1	0.8
DEN1058−15[d]	39	56.9	57.7	256.3	279.3	21.1
L3V	3.3	0.9	1.0	0.5	0.1	0.4
2M1146+22[e]	38	35.8	36.8	96.0	19.5	12.4
L3V	3.3	0.8	0.8	0.5	0.3	0.3
DEN1228−15[a]	31	48.6	49.4	224.0	143.3	21.5
L5V	3.1	1.9	1.9	1.3	0.3	0.8
SDSS1254−01	16	84.1	84.9	496.1	285.2	27.7
T2V	1.2	1.9	1.9	1.8	0.4	0.6
Kelu-1	30	52.4	53.6	285.0	272.2	25.2
L2V	3.3	2.0	2.0	1.0	0.2	0.9

TABLE 1—*Continued*

Object Sp. Type	No. Obs. ΔT(yr)	π(rel) (mas)	π(abs) (mas)	μ(rel) (mas yr^{-1})	P.A. (degrees)	$V_{\rm tan}$ (km s^{-1})
2M1328+21	25	30.1	31.0	481.1	152.9	73.6
L5V	3.3	3.8	3.8	1.8	0.2	9.0
2M1439+19	54	68.7	69.6	1295.3	288.3	88.2
L1V	3.4	0.5	0.5	0.2	0.1	0.6
T513-46546	53	93.2	94.4	62.9	203.0	3.2
M8.5V	3.2	0.5	0.6	0.4	0.3	0.0
2M1507−16	52	135.8	136.4	903.1	190.3	31.4
L5V	2.4	0.6	0.6	0.5	0.1	0.1
SDSS1624+00	28	90.7	91.5	383.2	269.6	19.9
T6V	2.2	2.3	2.3	1.9	0.5	0.5
2M1632+19	38	65.0	65.6	298.0	100.4	21.5
L8V	3.2	2.1	2.1	0.9	0.2	0.7
2M1658+70	30	53.1	53.9	346.0	205.1	30.4
L1V	2.0	0.7	0.7	0.9	0.1	0.4
GRH2208−20	170	23.9	24.7	691.7	197.4	132.7
M7.5V	7.1	0.5	0.5	0.2	0.1	2.7
2M2224−01	49	87.3	88.1	983.8	152.3	52.9
L4.5V	2.3	1.1	1.1	0.7	0.1	0.7

[a]Close binary with nearly equal magnitude components.
[b]Close binary with ΔI=0.62.
[c]Close binary with ΔI=1.27.
[d]Possible astrometric perturbation.
[e]Close binary with ΔI=0.31.

TABLE 2
PHOTOMETRY OF LATE-TYPE DWARFS/BROWN-DWARFS

Object Sp. Type	V	R_C	I_C	z^*	$J-H$	$H-K$	K	N_{obs}Opt N_{obs}IR
2M0015+35		19.35	17.22	16.46				-,2,2,2
L2V		0.01	0.02	0.02				-,-,-
BRI0021−02		17.42	15.16	14.36	0.74	0.54	10.58	-,2,2,2
M9.5V[a]		0.04	0.03	0.01	0.02	0.02	0.02	3,3,2
PC0025+04			19.79	18.68	0.73	0.44	14.91	-,-,2,2
M9.5Ve			0.07	0.02	0.02	0.03	0.04	9,9,9
2M0036+18	21.34	18.35	16.11	15.21	0.82	0.54	11.06	2,2,4,2
L3.5V	0.06	0.02	0.01	0.02	0.02	0.02	0.02	4,4,4
CTI0126+28	21.82	19.57	17.24	16.41	0.68	0.52	12.82	2,2,4,2
M8.5V	0.06	0.02	0.01	0.02	0.02	0.02	0.02	5,5,5
2M0149+29	21.25	18.94	16.81	16.02	0.87	0.56	11.96	2,2,4,2
M9.5Ve	0.05	0.02	0.01	0.02	0.02	0.02	0.02	4,4,4
DEN0205−11		20.98	18.44	17.21	0.96	0.56	13.06	-,3,2,3
L7V		0.04	0.02	0.05	0.02	0.02	0.04	4,4,4
T832−10443	20.82	18.51	16.13	15.37	0.65	0.44	11.96	2,2,3,2
M8V	0.05	0.01	0.01	0.01	0.02	0.05	0.02	3,3,3
LP412−31	19.21	16.98	14.70	13.96	0.68	0.44	10.67	1,2,3,2
M8V	0.02	0.01	0.01	0.01	0.02	0.02	0.02	3,3,2
2M0326+29			19.13	18.30	0.96	0.72	13.76	-,-,1,1
L3.5V			0.04	0.03	0.03	0.02	0.04	3,3,2
SDSS0330−00				17.93				-,-,-,1
L2V				0.03				-,-,-
2M0345+25	22.01	19.60	17.36	16.50	0.76	0.54	12.62	2,1,2,1
L0V[b]	0.08	0.04	0.01	0.02	0.04	0.02	0.02	3,3,3
SDSS0413−01				17.76				-,-,-,1
L0V				0.03				-,-,-
SDSS0539−00				16.70	0.84	0.58	12.49	-,-,-,2
L5V				0.02	0.05	0.05	0.04	1,1,1
2M0559−14			19.14	17.30				-,-,2,2
T5V			0.06	0.02				-,-,-
2M0746+20	19.87	17.40	15.11	14.29	0.74	0.47	10.49	1,4,4,3
L0.5V	0.06	0.01	0.01	0.01	0.02	0.02	0.03	2,2,1
2M0825+21		21.75	19.22	18.01	1.16	0.82	13.02	-,2,2,2
L7.5V		0.06	0.03	0.03	0.06	0.08	0.08	1,1,1
2M0850+10	>25.50	22.86	20.43	19.11	1.18	0.67	14.48	1,1,2,1
L6V		0.05	0.11	0.07	0.04	0.04	0.03	3,3,3
T213−2005	20.77	18.58	16.26	15.55	0.65	0.43	12.16	1,1,2,1
M:V	0.07	0.02	0.04	0.02	0.02	0.02	0.03	4.4,4
DEN1058−15		20.10	17.80	16.94	0.85	0.64	12.65	-,2,3,2
L3V		0.04	0.01	0.04	0.03	0.02	0.02	4,4,4

TABLE 2—*Continued*

Object Sp. Type	V	R_C	I_C	z^*	$J-H$	$H-K$	K	N_{obs}Opt N_{obs}IR
2M1112+35			18.32	17.48				-,-,2,2
GL417B; L4.5V			0.02	0.02				-,-,-
2M1146+22	22.65	20.14	17.85	17.01	0.90	0.62	12.59	1,1,3,2
L3V[b]	0.13	0.04	0.01	0.01	0.03	0.02	0.02	4,4,4
2M1217−03				19.54	−0.09[d]	0.30	15.70	-,-,-,1
T7.5				0.05	0.07	0.15	0.12	1,1,1
DEN1228−15		20.48	18.22	17.23	0.97	0.63	12.74	-,3,3,2
L5V		0.06	0.02	0.02	0.02	0.03	0.02	5,5,5
2M1237+65				19.62	−0.06[e]	−0.20	16.15	-,-,-,1
T6.5e				0.04	0.04	0.20	0.20	2,1,1
SDSS1254−01			19.76	18.05				-,-,2,2
T2			0.10	0.04				-,-,-
Kelu-1	21.77	19.10	16.94	16.18	0.92	0.66	11.80	2,1,3,2
L2V[c]	0.15	0.04	0.01	0.02	0.03	0.02	0.03	5,5,5
2M1328+21		22.48	20.09	18.99	1.08	0.71	14.13	-,1,2,4
L5V		0.04	0.06	0.05	0.03	0.03	0.02	5,5,5
SDSS1346−00					−0.11[f]			-,-,-,-
T6					0.04			4,-,-
LHS2828		16.10	14.05	13.74	0.56	0.33	11.09	-,2,2,2
M:V		0.02	0.01	0.01	0.04	0.02	0.02	3,3,3
GD165B				18.68	0.88	0.66	14.07	-,-,-,1
L4V				0.06	0.04	0.05	0.06	4,4,4
2M1439+1929	21.04	18.52	16.12	15.28	0.68	0.48	11.50	3,3,4,3
L1V	0.02	0.01	0.01	0.01	0.02	0.02	0.03	5,5,5
LHS3005		13.58	11.99	11.96	0.58	0.29	9.62	-,2,2,2
M3.5V		0.02	0.02	0.02	0.02	0.02	0.02	3,3,3
T513−46546	19.87	17.53	15.16	14.28				3,3,4,3
M8.5V	0.03	0.02	0.04	0.03				-,-,-
2M1507−16	22.9	19.04	16.65	15.62	0.90	0.52	11.40	1,2,3,2
L5V	0.5	0.03	0.03	0.01	0.02	0.02	0.02	4,4,4
2M1523+30			20.27	18.96	1.05	0.72	14.27	-,-,1,2
GL584C; L8V			0.11	0.06	0.04	0.06	0.04	3,3,3
2M1553+21	26.17	22.98						1,1,-,-
L5.5V	0.24	0.07						-,-,-
SDSS1624+00				18.89	−0.08[g]	0.01	15.45	-,-,-,4
T6				0.05	0.03	0.14	0.11	6,6,6
2M1632+19	>25.14	22.67	19.98	18.68	1.10	0.75	13.96	1,2,4,2
L8V		0.05	0.05	0.02	0.02	0.05	0.04	6,6,6
LHS429	16.81	14.71	12.28	11.73	0.58	0.37	8.83	3,1,3,2
vB8; M7V	0.02	0.02	0.02	0.01	0.02	0.02	0.02	3,3,3
2M1658+70		18.93	16.68	15.80				-,3,3,3
L1V		0.02	0.02	0.01				-,-,-

TABLE 2—*Continued*

Object Sp. Type	V	R_C	I_C	z^*	$J-H$	$H-K$	K	N_{obs}Opt N_{obs}IR
2M1726+15	24.49	21.62						1,1,-,-
L2V	0.26	0.03						-,-,-
L1421−36		11.38	10.16	10.21	0.63	0.22	7.93	-,1,1,1
G170-28; M:V		0.02	0.01	0.02	0.03	0.02	0.02	3,3,3
LHS3339		16.20	14.03	13.62	0.59	0.35	10.78	-,1,1,1
M5.5V		0.02	0.01	0.02	0.02	0.02	0.03	3,3,3
LHS3350		12.60	11.12	11.09	0.60	0.25	8.75	-,1,1,1
M:V		0.02	0.01	0.02	0.02	0.03	0.03	3,3,3
2M1841+31			19.26	18.70				-,-,2,2
L4Vpec			0.03	0.02				-,-,-
LHS3406	18.28	16.27	13.94	13.34	0.63	0.39	10.19	1,1,2,1
M5.5V		0.02	0.01	0.02	0.02	0.02	0.02	3,3,3
2M2101+17		23.25			...[h]			1,1,-,-
L7.5V		0.14						2,-,-
GRH2208−20	21.21	18.92	16.52	15.93	0.50	0.38	13.06	2,2,4,2
M7.5V	0.06	0.01	0.01	0.01	0.02	0.03	0.03	6,6,6
2M2208+29		22.02	19.73	18.96				-,1,1,1
L2Vpec		0.12	0.03	0.02				-,-,-
2M2224−01		20.29	18.02	17.08				-,4,4,5
L4.5V		0.03	0.01	0.04				-,-,-
2M2244+20			20.48	19.41				-,-,1,2
L6.5V			0.04	0.02				-,-,-

[a]Reported to be photometrically variable with low amplitude (Martín et al. 2001).
[b]Reported to be photometrically variable with low amplitude (Bailer-Jones & Mundt 2001).
[c]Reported to be photometrically variable with low amplitude (Clarke et al. 2002).
[d]$J = 15.82 \pm 0.04$.
[e]$J = 15.94 \pm 0.08$.
[f]$J = 15.74 \pm 0.04$.
[g]$J = 15.32 \pm 0.05$.
[h]$J = 16.95 \pm 0.05$.

TABLE 3
OTHER PARALLAX AND PHOTOMETRY DATA

Object Sp. Type	π(abs)	V	R_C	I_C	z^*	$J-H$	$H-K$	K	References
LHS102B	104.7			16.68		0.96	0.74	11.40	1, 15, 24
L5V	11.4			0.18		0.04	0.04	0.03	
2M0015+35						1.00	0.57	12.24	15
L2V						0.05	0.05	0.03	
BRI0021−02	86.6								6
M9.5V	4.0								
2M0235−23	47.0					0.69	0.67	12.32	2, 22
GJ1048B; L1V	1.0					0.16	0.13	0.08	
LP771−21	61.6			15.42		0.64	0.40	11.43	7, 8, 9
BRI0246−17; M8V	5.4			0.03		0.04	0.04	0.04	
SDSS0330−00					17.98	0.87	0.59	13.83	18, 21
L2V					0.04	0.06	0.06	0.05	
LP944−20[a]	201.4			14.16		0.70	0.50	9.52	7, 8, 9, 15
BRI0337−35; M9V	4.2			0.03		0.04	0.04	0.03	
SDSS0413−01					17.76	0.67	0.52	14.14	18, 21
L0V					0.02	0.07	0.07	0.06	
LHS191	58.4	18.32	16.24	13.95		0.58	0.33	10.69	3, 4
M6.5V	1.8	0.03	0.03	0.02		0.04	0.04	0.04	
SDSS0539−00					16.73	0.93	0.58	12.51	18, 21
L5V					0.01	0.04	0.04	0.03	
2M0559−14						0.15	0.07	13.61	19
T5V						0.05	0.06	0.05	
GL229B	173.2			19.92	17.69	−0.03	−0.07	14.42	2, 12, 26
T6.5V	1.1			0.14	0.13	0.07	0.07	0.05	
2M0825+21						1.33	0.74	13.05	15
L7.5V						0.06	0.06	0.04	
LHS2065	117.3	18.80	16.74	14.44		0.75	0.49	9.96	3, 4, 9
M9V	1.5	0.03	0.03	0.02		0.03	0.03	0.03	
2M0912+14	48.8					1.11	0.57	14.02	2, 20
GL337C; L8V	0.9					0.11	0.10	0.06	
2M1022+41	25.6					0.85	0.42	13.62	2, 20
HD89744B; L0V	0.7					0.06	0.07	0.05	
2M1112+35	46.0					1.10	0.78	12.69	2, 15
GL417B; L4.5V	0.9					0.06	0.06	0.05	
LHS2397a	70.0	19.57		14.95		0.72	0.43	10.75	3, 4, 5, 9
M8V	2.1	0.04		0.02		0.02	0.02	0.02	
LHS2471	70.3	17.97		13.69		0.59	0.35	10.30	3, 4
M6.5V	2.7	0.03		0.02		0.04	0.04	0.04	
2M1217−03				21.53		0.06[b]			14, 26
T7.5V				0.18		0.14			
BRI1222−12	58.6			15.74		0.70	0.46	11.34	5, 7, 8, 9
M9V	3.8			0.03		0.03	0.03	0.03	

TABLE 3—*Continued*

Object Sp. Type	π(abs)	V	R_C	I_C	z^*	$J-H$	$H-K$	K	References
2M1237+65 T6.5V				21.51 0.18		0.31[c] 0.16			21, 26
SDSS1254−01 T2V					18.00 0.04	0.84 0.05	0.21 0.07	13.83 0.06	18, 21
SDSS1346−00 T6V				21.03 0.18	19.27 0.05	−0.03 0.07	0.01 0.08	15.84 0.07	17, 26
LHS2828 M:V	36.5 1.0	17.70 0.02		14.06 0.02					3
GD165B L4V	31.7 2.5			19.16 0.07		1.01 0.06	0.64 0.05	14.13 0.05	1, 5, 6, 10, 11
LHS2924 M9V	90.8 1.3	19.58 0.04		15.21 0.02		0.70 0.03	0.47 0.03	10.70 0.03	3, 4, 9
LHS2930 M6.5V	103.8 1.4	17.88 0.03		13.31 0.02		0.60 0.04	0.37 0.04	9.72 0.04	3, 4
HD130948B L2:V	55.7 0.8					0.70 0.22	0.90 0.14	12.3 0.1	2, 25
HD130948C L2:V	55.7 0.8					0.60 0.22	1.00 0.14	12.6 0.1	2, 25
GL569Ba M8.5V	101.9 1.7					1.12[d] 0.10		10.02 0.08	2, 23
GL569Bb M9V	101.9 1.7					1.22[d] 0.10		10.43 0.08	2, 23
LHS3003 M7V	157.0 3.0	17.05 0.03	14.88 0.02	12.53 0.02		0.60 0.04	0.40 0.04	8.93 0.04	1, 4, 7
2M1457−21 GL570D; T8V	169.3 1.7			20.94 0.18	18.32 0.18	0.05 0.10	0.01 0.19	15.27 0.17	2, 16, 26
LHS3005 M:V	40.0 3.1	14.73 0.01							1
T513−46546 M8.5V						0.64 0.08	0.46 0.07	10.74 0.04	5, 9
T868-110639 M9V	61.2 4.7		18.19 0.03	15.79 0.03		0.73 0.03	0.47 0.03	11.36 0.03	5, 6, 8, 9
2M1523+30 GL584C; L8V	53.7 1.2					1.33 0.13	0.76 0.10	14.24 0.07	2, 15
2M1553+21 L5.5V					20.79 0.18	1.34 0.21	0.66 0.19	14.68 0.12	11
2M1620−04 GL618.1B; L2.5V	33.0 2.6					0.99 0.07	0.73 0.06	13.59 0.04	2, 20
SDSS1624+00 T6V				20.88 0.18	19.02 0.03	−0.03[e] 0.12			13, 26
LHS429 vB8; M7V	154.5 0.7	16.85 0.02		12.31 0.02					3
2M1658+70 L1V						0.77 0.04	0.62 0.04	11.92 0.03	21

TABLE 3—*Continued*

Object Sp. Type	π(abs)	V	R_C	I_C	z^*	$J-H$	$H-K$	K	References
2M1726+15 L2V				19.56 0.18		1.19 0.09	0.82 0.08	13.64 0.05	15, 26
L1421−36 G170−28; M:V	27.1 3.6	12.37 0.01							1
LHS3339 M5.5V	46.4 1.1	17.98 0.02		14.02 0.02					3
LHS3350 M:V	35.6 2.8	13.72 0.01							1
2M1841+31 L4Vpec						1.15 0.12	0.80 0.11	14.18 0.08	15
LHS3406 M:V	70.7 0.8	18.23 0.03		13.87 0.02					3
2M2101+17 L7.5V				20.73 0.18		1.17 0.24	0.66 0.24	15.04 0.19	15, 26
2M2208+29 L2Vpec						0.99 0.12	0.74 0.11	14.09 0.08	15
2M2224−01 L4.5V						1.25 0.04	0.79 0.04	12.02 0.03	15
2M2244+20 L6.5V						1.44 0.14	1.04 0.10	13.93 0.07	21

[a]Reported photometrically variable (Tinney & Tolley 1999).
[b]$J = 15.85 \pm 0.07$.
[c]$J = 16.03 \pm 0.09$.
[d]$J-K$ color, H was not observed.
[e]$J = 15.49 \pm 0.06$.

References.—

1. van Altena et al. (1995)
2. The Hipparcos and Tycho Catalogues (1997)
3. Monet et al. (1992)
4. Leggett (1992)
5. Tinney et al. (1993)
6. Tinney et al. (1995)
7. Tinney (1996)
8. Kirkpatrick et al. (1997b)
9. Leggett et al. (1998)
10. Becklin & Zuckerman (1988)
11. Kirkpatrick et al. (1999)
12. Leggett et al. (1999) (UKIRT system)
13. Burgasser et al. (2002)
14. Burgasser et al. (1999)
15. Kirkpatrick et al. (2000)
16. Burgasser et al. (2000b)
17. Tsvetanov et al. (2000) (UKIRT system)
18. Leggett et al. (2000b)
19. Burgasser et al. (2000a)
20. Wilson et al. (2001)
21. 2MASS Second Incremental Release
22. Gizis et al. (2001)
23. Lane et al. (2001)

TABLE 4
ESTIMATED MAGNITUDE DIFFERENCES

Filter	2M0746+20	2M0850+10	2M1146+22
V	0.75±0.08		0.40±0.10
R	0.62±0.04	1.50±0.25	0.31±0.04
I[a]	0.62±0.01	1.34±0.10	0.31±0.02
z^*	0.56±0.04	1.06±0.40	0.28±0.04
J	0.47±0.08	0.90±0.50	0.23±0.10
H	0.39±0.14	0.85±0.60	0.19±0.20
K	0.36±0.20		0.18±0.40

[a]Measured with HST (Reid et al. 2001b).

TABLE 5
EFFECTIVE TEMPERATURES

Star	Sp. Type	M_J	BC$_J$	$M_{\rm bol}$	$R/R_\odot$	$T_{\rm eff}$
LHS3339	M5.5	10.05	2.02	12.07	0.1308	2957 ± 70
LHS191	M6.5	10.43	2.05	12.48	0.1195	2813 ± 75
LHS3406	M5.5	10.46	2.03	12.49	0.1194	2811 ± 63
LHS2471	M6.5	10.47	2.05	12.52	0.1186	2800 ± 79
LHS429	M7	10.72	2.05	12.77	0.1129	2707 ± 63
LHS2930	M6.5	10.77	2.06	12.83	0.1118	2687 ± 65
T832−10443	M8	10.83	2.03	12.86	0.1112	2676 ± 66
LHS3003	M7	10.91	2.03	12.94	0.1096	2645 ± 70
LP412−31	M8	10.98	1.98	12.96	0.1092	2638 ± 67
GRH2208−20	M7.5	10.88	2.14	13.02	0.1080	2613 ± 73
LHS2397a	M8	11.13	1.97	13.10	0.1066	2583 ± 75
BRI1222−12	M9	11.34	1.99	13.33	0.1029	2496 ±100
BRI0021−02	M9.5	11.44	1.89	13.33	0.1029	2495 ± 86
CTI0126+28	M8.5	11.44	1.95	13.39	0.1020	2471 ± 69
2M0149+29	M9.5	11.63	1.77	13.40	0.1018	2467 ± 68
T868−110639	M9	11.49	1.95	13.44	0.1013	2451 ±112
LHS2065	M9	11.55	1.92	13.47	0.1009	2441 ± 66
LP771−21	M8	11.42	2.05	13.47	0.1009	2439 ±120
LHS2924	M9	11.66	1.99	13.65	0.0986	2367 ± 66
2M0345+25	L0	11.77	1.89	13.66	0.0985	2364 ± 69
Kelu-1	L2	12.03	1.65	13.68	0.0982	2354 ± 79
T513−46546	M8.5	11.72	2.05	13.77	0.0972	2319 ± 70
2M1658+70	L1	11.97	1.80	13.77	0.0972	2319 ± 66
2M0746+20A	L0.5	11.81	2.00	13.81	0.0967	2302 ± 67
PC0025+04	M9.5	11.78	2.03	13.81	0.0967	2302 ±143
2M1439+19	L1	11.87	2.01	13.88	0.0960	2273 ± 66
LP944−20	M9	12.24	1.98	14.22	0.0931	2138 ± 68
2M1112+35	L4.5	12.88	1.41	14.29	0.0926	2108 ± 67
2M1146+22A	L3	12.58	1.75	14.33	0.0923	2092 ± 71
2M0326+29	L3.5	12.90	1.58	14.48	0.0914	2031 ± 82
2M0036+18	L3.5	12.71	1.86	14.57	0.0909	1993 ± 64
DEN1058−15	L3	12.95	1.75	14.70	0.0903	1945 ± 65
LHS102B	L5	13.20	1.55	14.75	0.0901	1923 ±119
GD165B	L4	13.23	1.61	14.84	0.0897	1885 ± 94
2M1328+21	L5	13.38	1.54	14.93	0.0894	1853 ±127
2M2224−01	L4.5	13.77	1.31	15.08	0.0890	1792 ± 61
DEN1228−15	L5	13.56	1.67	15.23	0.0886	1734 ± 69
2M1507−16	L5	13.49	1.83	15.32	0.0885	1703 ± 60
DEN0205−11	L7	13.85	1.74	15.59	0.0882	1601 ± 63
2M0850+10A	L6	14.68	1.41	16.09	0.0880	1429 ± 92
2M1523+30	L8	14.79	1.46	16.25	0.0880	1376 ± 58
2M0825+21	L7.5	14.97	1.30	16.27	0.0880	1372 ± 54
2M1632+19	L8	14.89	1.49	16.38	0.0880	1335 ± 59

TABLE A1

FULL NAMES, COORDINATES, AND NOTES

Object	Coordinates RA (2000)	Dec	References Coords.	Chart
LHS102B[a]	00:04:33.9	−40:44:06	1	1
2MASSW J0015447+351603	00:15:44.7	+35:16:03	2	2
BRI 0021−0214	00:24:24.6	−01:58:22	3[bc]	3, 4
PCC0025+0447	00:27:41.4	+05:03:50	5[b]	5
2MASSW J0036159+182110	00:36:15.9	+18:21:10	2	2
CTI 012657.5+280202	01:27:39.2	+28:05:55	4[b]	4
2MASSW J0149090+295613	01:49:09.0	+29:56:13	6	6
DENIS−P J0205.4−1159[d]	02:05:29.0	−11:59:25	7	7
2MASSI J0235599−233120[e]	02:35:59.9	−23:31:20	8	99
LP771−21 = BRI 0246−1703	02:48:41.0	−16:51:19	9[f]	9
TVLM832−10443	02:52:26.4	+00:56:23	10[g]	10
LP412−31	03:20:58	+18:54.6	11[b]	4
2MASSW J0326137+295015	03:26:13.7	+29:50:15	12	12
SDSSp J033035.13−002534.5	03:30:35.1	−00:25:35	13	13
LP944−20 = BRI 0337−3535	03:39:34.6	−35:25:51	9[h]	9
2MASSP J0345432+254023	03:45:43.2	+25:40:23	12	12
SDSSp J041320.38−011424.9	04:13:20.4	−01:14:25	13	13
LHS191 = LP535−12	04:26:21	+03:36.5	14	15
SDSSp J053951.99−005902.0	05:39:52.0	−00:59:02	13	13
2MASSI J0559191−140448	05:59:19.1	−14:04:48	16	16
Gl229B	06:10:34.7	−21:51:46	17[i]	18
2MASSI J0746425+200032	07:46:42.5	+20:00:32	2	2
2MASSI J0825196+211552	08:25:19.6	+21:15:52	2	2
2MASSs J0850359+105716	08:50:35.9	+10:57:16	12	12
LHS2065 = LP666−9	08:53:36	−03:29.5	14	15
2MASSW J0912145+145940[j]	09:12:14.5	+14:59:40	19	19
TVLM213−2005	10:21:27.8	+50:55:03	10[g]	10
2MASSI J1022148+411426[k]	10:22:14.8	+41:14:26	19	19
DENIS−P J1058.7−1548[d]	10:58:46.5	−15:48:00	7	7
2MASSW J1112257+354813[l]	11:12:25.7	+35:48:13	2	2,20
LHS2397a = LP732−94	11:21:49.7	−13:13:07	9[m]	9
2MASSW J1146345+223053	11:46:34.5	+22:30:53	12	12
LHS2471 = LP553−59	11:53:53	+07:00.3	14	15
2MASSW J1217111−031113	12:17:11.1	−03:11:13	21	21
BRI 1222−1222	12:24:52.4	−12:38:31	9[n]	9
DENIS−P J1228.2−1547[d]	12:28:13.8	−15:47:11	7	7
2MASSW J1237392+652615	12:37:39.2	+65:26:15	21	21
SDSS J125453.90−012247.4	12:54:53.9	−01:22:47	22	22
Kelu-1	13:05:40.2	−25:41:06	23[o]	23
2MASSW J1328550+211449	13:28:55.0	+21:14:49	12	12
SDSSp J134646.45−003150.4	13:46:46.5	−00:31:50	24	24
LHS2828 = LP499−5	13:57:02	+08:30.1	14	15
GD165B	14:24:39.3	+09:17:15	25[bp]	4
LHS2924 = LP271-25	14:28:42	+33:10.6	14	15
LHS2930 = LP98-79	14:30:40	+59:43.2	14	15
2MASSW J1439284+192915	14:39:28.4	+19:29:15	12	12
HD130948BC[q]	14:50:15.8	+23:54:43	17	26
Gl569B[r]	14:54:29.3	+16:06:04	17	27
LHS3003 = LP914-54	14:56:38	−28:09.8	14	15
2MASSW J1457150−212148[s]	14:57:15.0	−21:21:48	28	28
LHS3005 = G136−39	14:57:20	+14:59.0	14	15
TVLM513−46546	15:01:08.2	+22:50:02	10[g]	10
2MASSW J1507476−162738	15:07:47.6	−16:27:38	2	2
TVLM868−110639	15:10:17.1	−02:36:07	10[b]	10
2MASSW J1523226+301456[t]	15:23:22.6	+30:14:56	2	2,20
2MASSW J1553214+210907	15:53:21.4	+21:09:07	12	12
2MASSW J1620261−041631[u]	16:20:26.1	−04:16:31	19	19
SDSS J162414.37+002915.6	16:24:14.4	+00:29:16	29	29
2MASSW J1632291+190441	16:32:29.1	+19:04:41	12	12
LHS429 = vB8	16:55:34	−08:23.6	14	15
2MASSW J1658038+702702	16:58:03.8	+70:27:02	99	99
L1421−36 = G170−28 = LP332−9	17:14:42	+26:56.0	11	30
2MASSI J1726000+153819	17:26:00.0	+15:38:19	2	2
LHS3339 = LP102−330	17:55:33	+58:24.4	14	15
LHS3350 = G182−34	18:01:16	+35:35.9	14	15
2MASSW J1841086+311727	18:41:08.6	+31:17:27	12	12
LHS3406 = LP229−30	18:43:22	+40:40.4	14[v]	15

TABLE A1—*Continued*

Object	Coordinates RA (2000)	Dec	References Coords.	Chart
2MASSW J2101154+175658	21:01:15.4	+17:56:58	12	12
2MASSW J2208136+292121	22:08:13.6	+29:21:21	12	12
GRH 2208−2007	22:10:50.0	−19:52:13	31[t]	9[w]
2MASSW J2224438−015852	22:24:43.8	−01:58:52	2	2
2MASSW J2244316+204343	22:44:31.6	+20:43:43	99	99

[a]Faint companion to LHS102 = LP988−102 = GJ1001.
[b]Coordinates precessed from 1950.0 values given in Ref. to equinox 2000.0 (but *not* epoch 2000.0).
[c]Coordinates for Epoch 1989.8. See remarks in Ref.4 regarding confusion with earlier discovery of this object by Luyten.
[d]In original discovery paper the name employed used "DBD" rather than "DENIS−P." However, the "DENIS−P" became standard nomenclature for such objects discovered in the "Minisurvey" from DENIS (see Tinney et al. 1998). In the 1997 and 1998 papers the names included the RA portion only to integer minutes of time; in various later papers (e.g., K99; K00), the name includes decimal minutes of time.
[e]Faint companion to CD−24°1154 = HD16270 = GJ1048.
[f]Coordinates for Epoch 1988.9.
[g]2000.0 coordinates from SIMBAD.
[h]Coordinates for Epoch 1976.9.
[i]Faint companion to BD−21°1377 = HD42581 = LHS1827 = Gliese 229. Coordinates are for Gl229A at Epoch 1991.25. The separation and offset to Gl229B is 7.7 arcsec at 163.7 degrees (Ref.18).
[j]Faint companion to BD+15°2003AB = HD79096AB = LHS2114 = Gliese 337AB.
[k]Faint companion to HR4067 = BD+41°2076 = HD89744.
[l]Faint companion to BD+36°2162 = HD97334 = Gliese 417.
[m]Coordinates for Epoch 1985.4.
[n]Coordinates for Epoch 1984.3.
[o]Coordinates for Epoch 1993.2.
[p]Coordinates for GD165A at Epoch 1988.7. GD165B is located 0.7"W and 4.2"S of GD165A (Ref.25).
[q]Pair of faint companions to HD130948 = BD+24°2786 = HR5534 = Gliese 564. Coordinates are for HD130948A. The separation and offset to HD130948BC is 3 arcsec at 110 degrees (Ref.26).
[r]Pair of faint companions to G138−28 = BD+16°2708 = Gliese 569. Coordinates are for Gl569A. The separation and offset to Gl569B is 5 arcsec at 18 degrees (Ref.27).
[s]Faint companion to the triple system composed of BD−20°4125 = HD131977, and BD−20°4123AB = HD131976AB, or Gliese 570ABC.
[t]Faint companion to BD+30°2653AB = HD137107/8 = Gliese 584AB.
[u]Faint companion to Gliese 618.1.
[v]The 2000 RA coordinate given in LHS Catalogue (18:42:22) seems to be incorrect by approximately 1.0 min. The more correct value is quoted here.
[w]Coordinates for Epoch 1976.0. As noted in Ref.9, the chart given in Ref.31 is incorrect.

REFERENCES.—

1. Goldman et al. (1999)
2. K00
3. Irwin et al. (1991)
4. Kirkpatrick et. al. (1995)
5. Schneider et al. (1991)
6. Liebert et al. (1999)
7. Delfosse et al. (1997)
8. Gizis et al. (2001)
9. Tinney (1996)
10. Tinney et al. (1995)
11. Luyten (1979a - NLTT)
12. K99
13. Fan et al. (2000)
14. Luyten (1979b - LHS)
15. Luyten & Albers (1979 - LHS Atlas)
16. Burgasser et al. (2000a)
17. The Hipparcos and Tycho Catalogues, Vol.6, (1997)
18. Golimowski et al. (1998)
19. Wilson et al. (2001)
20. Kirkpatrick et al. (2001)
21. Burgasser et al. (1999)
22. Leggett et al. (2000b)
23. Ruiz et al. (1997)
24. Tsvetanov et al. (2000)
25. Becklin & Zuckerman (1988)
26. Potter et al. (2002)
27. Forrest et al. (1988)
28. Burgasser et al. (2000b)
29. Strauss et al. (1999)
30. Giclas et al. (1964)
31. Gilmore et al. (1985)
99. Unpublished